AD-A072 085 NATIONAL AVIATION FACILITIES EXPERIMENTAL CENTER ATL--ETC F/G 17/9
NUMERICAL STUDIES OF CONVERSION AND TRANSFORMATION IN A SURVEIL--ETC(U)
APR 79 R G MULHOLLAND, D W STOUT

UNCLASSIFIED FAA-NA-79-17 NL

| OF |
ADA
072085

END
DATE
FILMED
9-79
DDC

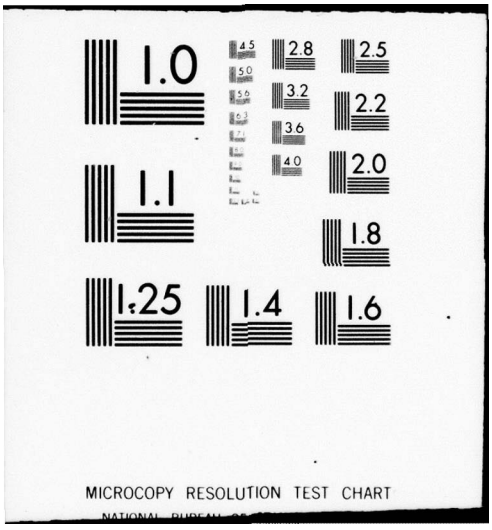
1.0
1.1
1.25
1.4
1.6
1.8
2.0
2.2
2.5
2.8
3.2
3.6
4.0
4.5
5.0
5.6
6.3
MICROCOPY RESOLUTION TEST CHART

Report No. FAA-NA-79-17

LEVEL II

NUMERICAL STUDIES OF CONVERSION AND TRANSFORMATION IN A SURVEILLANCE SYSTEM EMPLOYING A MULTITUDE OF RADARS - PART I

R.G. Mulholland

D.W. Stout

APRIL 1979

NAFEC REPORT

Prepared for

U. S. DEPARTMENT OF TRANSPORTATION

FEDERAL AVIATION ADMINISTRATION

National Aviation Facilities Experimental Center

Atlantic City, New Jersey 08405

NOTICE

The United States Government does not endorse products or manufacturers. Trade or manufacturer's names appear herein solely because they are considered essential to the object of this report.

Technical Report Documentation Page

1. Report No.	2. Government Accession No.	3. Recipient's Catalog No.
FAA-NA-79-17		

4. Title and Subtitle
Numerical Studies of Conversion and Transformation in a Surveillance System Employing a Multitude of Radars, Part I

AD72086

5. Report Date
Apr[illegible]79

6. Performing Organization Code
ANA-220

7. Author(s)
R. G. Mulholland and D. W. Stout

8. Performing Organization Report No.
FAA-NA-79-17

9. Performing Organization Name and Address
Federal Aviation Administration
National Aviation Facilities Experimental Center
Atlantic City, New Jersey 08405

10. Work Unit No. (TRAIS)

11. Contract or Grant No.
975-200-10A

12. Sponsoring Agency Name and Address
U.S. Department of Transportation
Federal Aviation Administration
National Aviation Facilities Experimental Center
Atlantic City, New Jersey 08405

13. Type of Report and Period Covered
NAFEC

14. Sponsoring Agency Code
ANA-1

15. Supplementary Notes

12 48p.

16. Abstract
Conversion error is considered in the application of stereographic projection to the planar representation of targets in multiple radar surveillance systems. The error is treated as the separation of images in a local radar plane of target position (in terms of altitude, azimuth, and slant range) under ideal mapping formulae and system implementations thereof. These images are viewed as elements of a complex plane in which the center of coordinates represents the radar site. Thus, conversion error can be expressed in terms of a range error equal to the difference in moduli of two complex numbers and an angle error equivalent to the difference between the arguments of the same numbers. As the image of target position under ideal conversion traverses a circle centered on the origin of coordinates, both the angle error and the range error oscillate about median values. The amplitude of each oscillation increases with the radius of the circle. In addition, the median range error is strongly dependent upon the radius of the circle. On the other hand, the median angle error is identically zero. An error correction method and a commonly used minimax technique are considered as alternative means for controlling conversion error.

17. Key Words	18. Distribution Statement
Coordinate Conversion and Transformation, Stereographic Projection, Multiple Radar Surveillance System	Document is available to the U.S. public through the National Technical Information Service, Springfield, Virginia 22161

19. Security Classif. (of this report)	20. Security Classif. (of this page)	21. No. of Pages	22. Price
Unclassified	Unclassified	47	

Form DOT F 1700.7 (8-72) Reproduction of completed page authorized

240 550

METRIC CONVERSION FACTORS

Approximate Conversions to Metric Measures

Symbol	When You Know	Multiply by	To Find	Symbol
	LENGTH			
in	inches	*2.5	centimeters	cm
ft	feet	30	centimeters	cm
yd	yards	0.9	meters	m
mi	miles	1.6	kilometers	km
	AREA			
in^2	square inches	6.5	square centimeters	cm^2
ft^2	square feet	0.09	square meters	m^2
yd^2	square yards	0.8	square meters	m^2
mi^2	square miles	2.6	square kilometers	km^2
	acres	0.4	hectares	ha
	MASS (weight)			
oz	ounces	28	grams	g
lb	pounds	0.45	kilograms	kg
	short tons (2000 lb)	0.9	tonnes	t
	VOLUME			
tsp	teaspoons	5	milliliters	ml
Tbsp	tablespoons	15	milliliters	ml
fl oz	fluid ounces	30	milliliters	ml
c	cups	0.24	liters	l
pt	pints	0.47	liters	l
qt	quarts	0.95	liters	l
gal	gallons	3.8	liters	l
ft^3	cubic feet	0.03	cubic meters	m^3
yd^3	cubic yards	0.76	cubic meters	m^3
	TEMPERATURE (exact)			
°F	Fahrenheit temperature	5/9 (after subtracting 32)	Celsius temperature	°C

*1 in = 2.54 (exactly). For other exact conversions and more detailed tables, see NBS Misc. Publ. 286, Units of Weights and Measures, Price $2.25, SD Catalog No. C13.10:286.

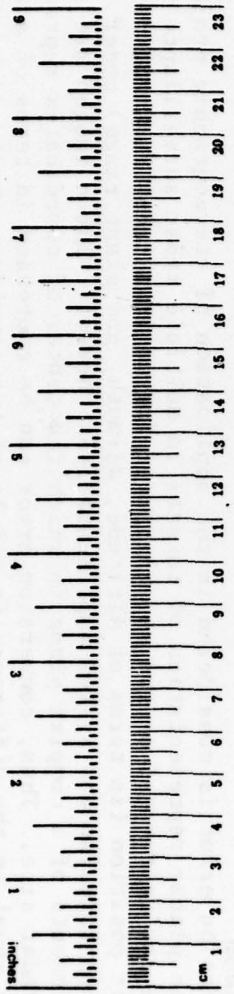

Approximate Conversions from Metric Measures

Symbol	When You Know	Multiply by	To Find	Symbol
	LENGTH			
mm	millimeters	0.04	inches	in
cm	centimeters	0.4	inches	in
m	meters	3.3	feet	ft
m	meters	1.1	yards	yd
km	kilometers	0.6	miles	mi
	AREA			
cm^2	square centimeters	0.16	square inches	in^2
m^2	square meters	1.2	square yards	yd^2
km^2	square kilometers	0.4	square miles	mi^2
ha	hectares (10,000 m^2)	2.5	acres	
	MASS (weight)			
g	grams	0.035	ounces	oz
kg	kilograms	2.2	pounds	lb
t	tonnes (1000 kg)	1.1	short tons	
	VOLUME			
ml	milliliters	0.03	fluid ounces	fl oz
l	liters	2.1	pints	pt
l	liters	1.06	quarts	qt
l	liters	0.26	gallons	gal
m^3	cubic meters	35	cubic feet	ft^3
m^3	cubic meters	1.3	cubic yards	yd^3
	TEMPERATURE (exact)			
°C	Celsius temperature	9/5 (then add 32)	Fahrenheit temperature	°F

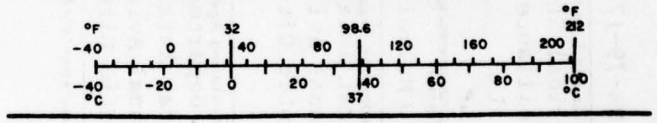

PREFACE

Acknowledgment is given to R. E. Lefferts who suggested the topic of this report. A great deal of benefit was derived from many conversations with him on the subject of multiple radar data processing systems. F. R. Mullin was also available for discussion. His extensive experience with the National Airspace System was a valuable source of information.

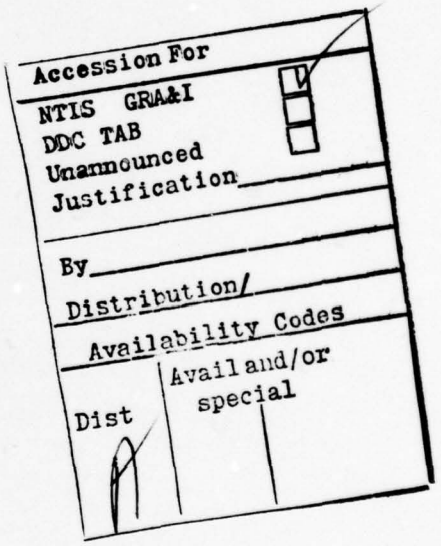

TABLE OF CONTENTS

LIST OF ILLUSTRATIONS

EXECUTIVE SUMMARY

This two-part paper is concerned with the application of stereographic projection to long-range surveillance systems employing a multitude of radars. It is an extension of earlier investigations of the same subject in connection with the Semi-Automatic Ground Environment System (SAGE) and the National Airspace System (NAS). Reconsideration of the topic at this time is appropriate in view of current trends in the air traffic control (ATC) community. Among these are improved accuracy of modern sensors now being contemplated as replacements for present operational radars, and the necessity of providing reliable forecasts of target position over long time intervals in advanced ATC functions such as Conflict Alert. A fundamental consideration is whether errors introduced by system implementation of stereographic projection are compatible with the quality of data offered by new radar technology and the objectives of advanced ATC services. Accordingly, this paper deals with the origin of such errors, the size of the errors, and alternative methods of controlling the errors in the context of the reference ellipsoid, a mathematical representation of the equipotential surface of the gravity field at mean sea level.

In long-range surveillance systems, target positions are represented by points in a so-called master plane. These points are obtained by mapping target altitude, azimuth, and slant range into the master plane. If the mapping is equivalent to stereographic projection of target latitude and longitude into the plane, then the master plane representation of a target is invariant to the radar from which azimuth and slant range are measured (provided, of course, that there is no measurement error). In a strict theoretical sense, it is possible to achieve such an equivalence by means of a two-stage procedure. First, there is a conversion of target altitude together with target azimuth and slant range relative to any given radar site into a point on a plane unique to the radar. This is followed by a transformation that carries points in the local radar plane into points on the master plane. In practice, exact duplication of ideal conversion and transformation processes is not possible. As a result, there are conversion errors and transformation errors, and these adversely affect the master plane representation of targets.

Part I of the paper treats conversion error; i.e., the distance between images in the local radar plane of target position (in terms of altitude, azimuth, and slant range) under ideal conversion and system implementations thereof. These images are viewed as elements of a complex plane in which the center of coordinates represents the radar site. Thus, conversion error can be expressed in terms of a range error equal to the difference in moduli of two complex numbers and an angle error equivalent to the difference between the arguments of the same numbers. As the image of target position under ideal conversion traverses a circle centered on the origin of coordinates, both the angle error and the range error oscillate about median values. The amplitude of each oscillation increases with the radius of the circle. In addition,

the median range error is strongly dependent upon the radius of the circle. On the other hand, the median angle error is identically zero.

In the case where error control is effected by commonly accepted procedures, the angle error is less than 0.0056° under standard operational conditions. Moreover, the amplitude of the range error is upper bounded by 0.02 nautical mile, whereas the median range error can exceed 0.2 nautical mile. However, at least from the theoretical point of view, there is another method of error control capable of substantially eliminating the median range error without disturbing the amplitudes of the angle and range error oscillations. Needless to say, the reduction in error attainable with the alternative method is significant. While the practicality of the approach in the present environment is a moot question, the method does offer some interesting possibilities in the context of a future replacement for the NAS computer system.

Part II of the paper deals with transformation error; i.e., the distance between images in the master plane of the same element in the local radar plane under ideal transformation and polynomial approximations thereof. Tight upper and lower bounds are derived for the error generated by the nth-order approximation to the ideal transformation equation under parameter constraints consistent with the size of coverage areas associated with current air traffic control centers (ARTCC's) and the range of operational radars. In the case of the first-order approximation, the error can exceed 0.8 nautical mile, whereas the error involved in the second-order approximation is less than 8 meters. Clearly, from the standpoint of error control, the first order approximation is far less desirable than the second-order approximation. However, the error introduced by the nth-order approximation is dependent upon the location of the radar site from which positional information is collected as well as the distance between the target and the radar. Thus, as in the current ATC environment, by using both approximations, it is possible to take advantage of the simplicity of the first-order approximation without accepting an intolerable transformation error.

Although not altogether obvious, the transformation process is intimately connected with the so-called magnification factor. This is just the amount by which the length of an infinitesimal arc on the reference ellipsoid is amplified under stereographic projection into the master plane. The factor varies with the position of the arc on the reference ellipsoid. For purposes of convenience, as well as prediction accuracy, it is desirable that the magnification factor be close to unity over the coverage region of the surveillance system. In Part II, practical procedures for accomplishing this desideratum (other than those in current use) are discussed. These procedures provide an upper bound on the deviation of the magnification factor from unity over the coverage region. The bound is dependent on coverage region size. For example, if the maximum distance between any two points in a coverage region is on the order of 1,100 nautical miles, then it is possible to keep the deviation below 0.004. As a result, the magnification factor must fall between 0.996 and 1.004 over the entire coverage region. In the case of coverage regions with diameters less than 1,100 nautical miles, smaller bounds on the deviation from unity are attainable.

In conclusion, it is emphasized that this investigation has been conducted under the assumption that sensor measurements are exact and data processing is carried out with infinite precision. In practice, this is not the case. Receiver front-end noise exists, range and azimuth measurements are quantized before being passed on to the central processor, trigonometric functions and other standard mathematical relationships are approximated in various ways by system hardware and software, and multiplication and addition are carried out using finite precision arithmetic. All of these contribute to error, and we have no reason to believe the effect upon conversion and transformation is inconsequential. In this sense, the results of the paper should be viewed as representative of these processes under ideal operating conditions.

1. INTRODUCTION

This is the first part of a two-part paper dealing with two-dimensional representations of target position from measurements of altitude, slant range, and azimuth in a multiple radar data processing system. It is concerned with the case in which such representations are realized by means of stereographic projection. Assuming that the mean sea level surface of the earth is an ellipsoid of revolution, this technique can be used to establish a unique relationship between points on a plane and orthogonal projections of points in space onto the earth's surface. The latter can be determined from measurements of slant range, azimuth, and altitude above mean sea level. Thus, in the case of targets at the same latitude and longitude but different altitudes, such measurements are mapped into a single point on the plane. In this way, data obtained from many radars can be used to assemble a single planar representation of positions of aircraft and other targets in three-dimensional space.

The mapping of target positions onto a single plane can be viewed as a two-stage procedure. First, there is a conversion of target altitude together with target slant range and azimuth relative to any given radar site into a point on a local radar plane. This is followed by a transformation that carries points in the local plane into points on a single master plane. Thus, there are as many local planes as there are radars, and each of these is mapped into the master plane to establish the final planar representation of positions of targets within the coverage region of the overall surveillance system.

Ideally, conversion involves a determination of the orthogonal projection of target position on the ellipsoidal representation of the mean sea level surface of the earth, a mapping of the projection onto a so-called conformal sphere, and stereographic projection of the spherical surface onto the local radar plane. Transformation, in the ideal sense, is realized by a bilinear transformation that takes the local plane into the master plane. When carried out in this fashion, the process of conversion and transformation is equivalent to the three steps of conversion alone with the exception that the local and master planes are the same. Thus, under ideal conversion and transformation, the planar representation of a target is invariant to the radar with respect to which slant range and azimuth are measured.

Unfortunately, in practice, it is difficult to realize the ideal forms of conversion and transformation. As a result, modifications of these procedures are encountered in operational systems. Here and in the sequel (reference 7), we will investigate differences between images of a target under ideal and approximate conversion procedures as well as differences between images of a point on the local radar plane under the ideal bilinear transformation and polynomial approximations thereof. While the subject is far from new (references 1, 2, and 3), numerical results are scarce, conversion differences are expressed by formulae derived from spherical earth models, and optimization of differences is defined in terms of minimax criteria applied to targets above the radar platform plane. Objectives of this investigation are

to assemble a comprehensive and yet concise picture of pertinent theoretical results applicable to an ellipsoidal earth model, to provide numerical results characterizing differences between ideal procedures and those encountered in practice, and to consider alternative methods for maintaining such differences within tolerable bounds.

Our study relies heavily upon the work of Flax (reference 4), which is an elegant unified treatment of theoretical aspects of conversion and transformation based upon the assumption of a spherical earth. Here, his results are combined with the concept of a conformal sphere (reference 5) to provide mathematical frameworks for both ideal and approximate forms of conversion and transformation in the context of an ellipsoidal earth model. In addition, numerical results exhibiting the differences between the exact and approximate conversion procedures are examined, and attention is directed to the problem of reducing such differences. Numerical investigations of transformation are left to the sequel.

The next section summarizes essential features of geodetic coordinates used in future developments. The relationship between geodetic coordinates and measurements of slant range, azimuth, and altitude is discussed in section 3. Section 4 describes the relationship between conformal and geodetic latitudes and exhibits the mathematical formulas by which the surface of a conformal sphere can be stereographically projected onto a plane. In addition, the connection is shown between stereographic projection and the planar representation of targets in multiple radar surveillance systems. The details of conversion are presented in section 5. In section 6, the differences between the results of ideal conversion and those achieved by approximations employed in operational systems are defined in precise terms. Section 7 provides numerical results that characterize the behavior of these differences for some realistic target positions and radar site locations in the case where error control is effected by means of a minimax procedure. An alternative procedure for controlling errors is discussed in section 8. Concluding remarks appear in section 9.

2. GEODETIC COORDINATES

The gravity field of the earth is the result of two forces, the centrifugal force due to the earth's rotation and the force of mass attraction between the earth and other bodies. It can be described in terms of equipotential surfaces, and the force of gravity is perpendicular to such surfaces. The equipotential surface at mean sea level is called the geoid. It is irregular and hence unsuitable as a basis for a coordinate system. The geoid can be closely approximated by an ellipsoid of revolution called the reference ellipsoid. This geometry is often used for purposes of navigation, gravity computations, etc.

An ellipsoid is illustrated in figure 1. It has a semimajor axis of length a (the equatorial radius) and a semiminor axis of length b (the polar radius). In the case of the reference ellipsoid (reference 6),

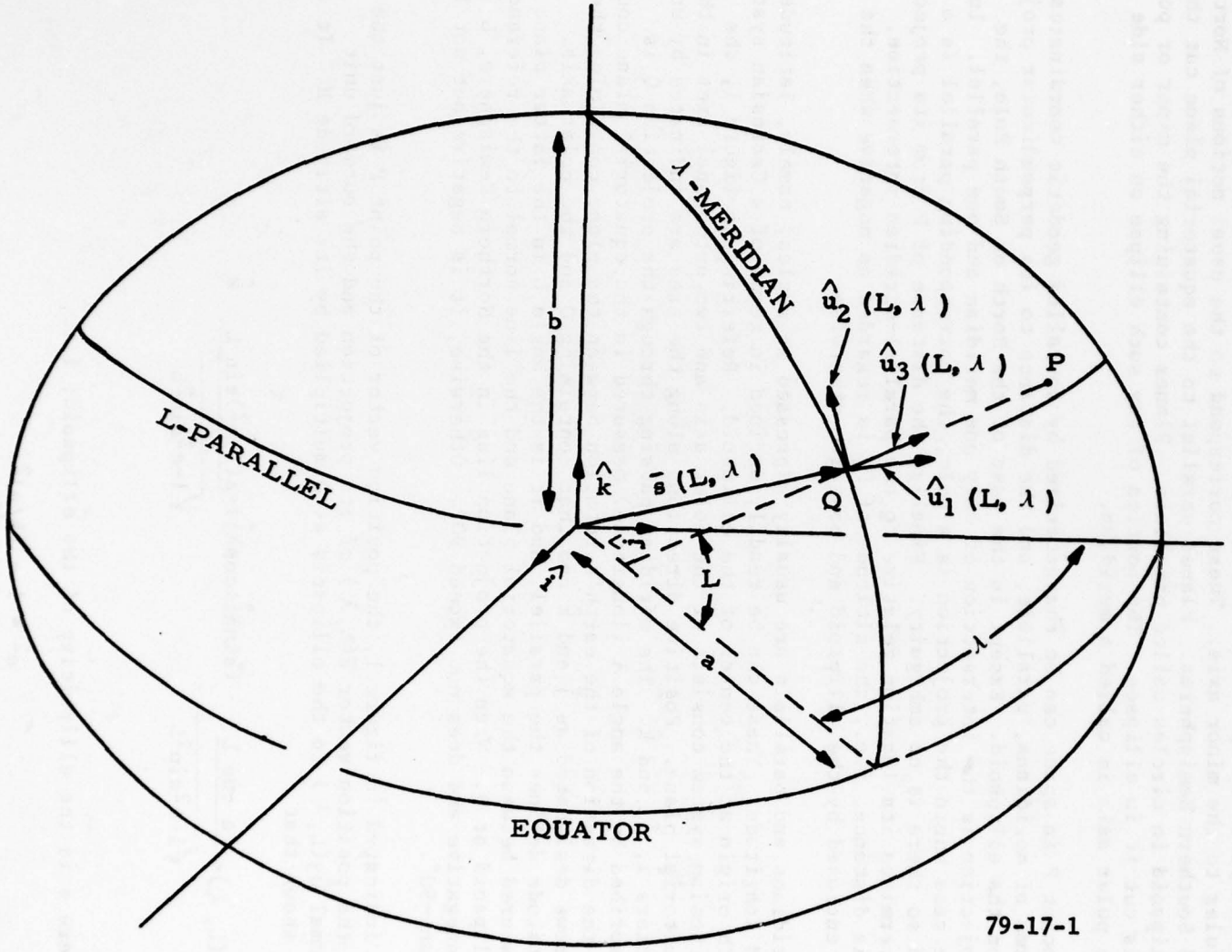

FIGURE 1. REFERENCE ELLIPSOID

$a = 6{,}378{,}388$ meters and $b = 6{,}356{,}912$ meters.

The direction of the earth's rotation is indicated by the arrowhead (pointing north) on the minor axis in conjuntion with the usual right-hand rule. The ellipsoid is split into halves by a plane (the equatorial plane) perpendicular to the minor axis. These correspond to the usual notions of Northern and Southern Hemispheres. Planes parallel to the equatorial plane cut the ellipsoid in circles called parallels. Planes containing the minor or polar axis cut it in ellipses. The portion of any such ellipse on either side of the polar axis is called a meridian.

A point P in space can be characterized by so-called geodetic coordinates in terms of meridians, parallels, and the distance to its perpendicular projection Q on the ellipsoid. Except in the case of the North or South Pole, the projection is the intersection of only one meridian and one parallel. In the case where the projection is a pole, the corresponding parallel is a point and so there is no ambiguity. Finally, the distance of P from its projection determines its location relative to the parallel-meridian intersection. This distance, i.e., the altitude of P, is regarded as negative when the point is enclosed by the ellipsoid and positive otherwise.

Meridians and parallels are usually expressed as angles, namely, latitude and longitude. These can be readily defined in terms of a Cartesian system with origin at the center of the ellipsoid. Referring to figure 1, the Cartesian system consists of the polar axis and two orthogonal axes in the equitorial plane. Positive directions along the axes are indicated by unit vectors $\hat{i}$, $\hat{j}$, and $\hat{k}$. The meridian passing through the projection Q is described by the angle λ (longitude) measured in the equatorial plane counter to the direction of the earth's rotation between the plane containing the arrows designated as $\hat{j}$ and $\hat{k}$ and that containing Q and the polar axis. Latitude defines the parallel, and it is the angle L in the latter plane measured between the equatorial plane and the line normal to the reference ellipsoid at Q. When the projection lies in the Northern Hemisphere, L is nonnegative and does not exceed 90°. Otherwise, it is negative but not less than -90°.

As indicated in figure 1, the position vector of the point P is just the sum of the position vector $\bar{s}(L, \lambda)$ of its projection and the outward unit normal $\hat{u}_3(L, \lambda)$ to the ellipsoid at Q multiplied by its altitude H. It can be shown that

$$\bar{s}(L, \lambda) = \frac{a \cos L}{\sqrt{1-e^2 \sin^2 L}} (\sin\lambda \hat{i} + \cos\lambda \hat{j}) + \frac{a(1-e^2)\sin L}{\sqrt{1-e^2 \sin^2 L}} \hat{k} \qquad (1)$$

where e is the ellipticity of the ellipsoid; i.e.,

$$e^2 = 1 - (b/a)^2. \qquad (2)$$

Moreover, from figure 1, it is not difficult to see that

$$\hat{u}_3(L,\lambda) = \cos L\,(\sin\lambda\,\hat{i} + \cos\lambda\,\hat{j}) + \sin L\,\hat{k}. \tag{3}$$

Thus, the position vector of point P in terms of its latitude, longitude, and altitude can be expressed as

$$\bar{s}(L,\lambda) + H\,\hat{u}_3(L,\lambda) \tag{4}$$

In later sections, we shall find it convenient to refer to unit vectors $\hat{u}_1(L,\lambda)$ and $\hat{u}_2(L,\lambda)$. In figure 1, these are pictured as lying in the plane tangent to the surface of the reference ellipsoid at Q. In addition, the vector $\hat{u}_2(L,\lambda)$ lies in the plane defined by the λ-meridian and is directed from the South toward the North Pole. Inspection of figure 1 shows that

$$\hat{u}_2(L,\lambda) = -\sin L \sin\lambda\,\hat{i} - \sin L \cos\lambda\,\hat{j} + \cos L\,\hat{k}. \tag{5}$$

The remaining vector is defined by the cross product

$$\begin{aligned}\hat{u}_1(L,\lambda) &= \hat{u}_2(L,\lambda) \times \hat{u}_3(L,\lambda) \\ &= -\cos\lambda\,\hat{i} + \sin\lambda\,\hat{j}.\end{aligned} \tag{6}$$

It can be viewed as lying in the plane defined by the L-parallel and pointing along the parallel in the direction of the earth's rotation. In the degenerate case where the projection of P is either the North or the South Pole, it is sufficient to consider $\hat{u}_1(L,\lambda)$ and $\hat{u}_2(L,\lambda)$ to be any orthogonal pair of unit vectors such that

$$\hat{u}_3(L,\lambda) = \hat{u}_1(L,\lambda) \times \hat{u}_2(L,\lambda). \tag{7}$$

3. SLANT RANGE AND AZIMUTH

Consider a radar at altitude H_R above the reference ellipsoid at latitude L_s and longitude λ_s. Let (L, λ, H) represent the geodetic coordinates of some target. The position vector of the radar site can be expressed as

$$\bar{r}(L_s, \lambda_s, H_R) = \bar{s}(L_s, \lambda_s) + H_R\,\hat{u}_3(L_s, \lambda_s), \tag{8}$$

and the position vector $\bar{r}(L, \lambda, H)$ of the target can be written in an analogous form. As shown in figure 2,

$$\bar{t}(L,\lambda, H) = \bar{r}(L, \lambda, H) - \bar{r}(L_s,\lambda_s, H_R) \tag{9}$$

can be viewed as an arrow drawn from the radar site to the target.

Obviously, the magnitude S of the vector $\bar{t}(L, \lambda, H)$ is just the slant range of the target. We can also express target azimuth as a function of this vector and the unit vectors $\hat{u}_1(L_s, \lambda_s)$ and $\hat{u}_2(L_s, \lambda_s)$. In order that the expression yield an angle measured in the plane of the radar platform in accordance with the usual notions of azimuth, it is essential that the axis of rotation of the platform be normal to the surface of the ellipsoid at $(L_s, \lambda_s, 0)$. Thus, in figure 2, the axis of rotation is depicted as coincident with the unit normal vector $\hat{u}_3(L_s, \lambda_s)$. As shown in the same figure, it is assumed that the platform rotates in the direction from $\hat{u}_2(L_s, \lambda_s)$ to $\hat{u}_1(L_s, \lambda_s)$ in accordance with the right-hand rule used in conjunction with the negative of $\hat{u}_3(L_s, \lambda_s)$. With this understanding, we define the target azimuth θ in terms of the orthogonal projection of $\bar{t}(L, \lambda, H)$ into the plane tangent to the ellipsoid at the orthogonal projection of the radar site, i.e., $(L_s, \lambda_s, 0)$. More precisely, θ is the angle measured in the tangent plane (which is parallel to the radar platform plane) from $\hat{u}_2(L_s, \lambda_s)$ in the direction of platform rotation to the projection of $\bar{t}(L, \lambda, H)$. In terms of vector dot products,

$$\sin\theta = \frac{1}{d}[\bar{t}(L, \lambda, H) \cdot \hat{u}_1(L_s, \lambda_s)] \tag{10}$$

and

$$\cos\theta = \frac{1}{d}[\bar{t}(L, \lambda, H) \cdot \hat{u}_2(L_s, \lambda_s)] \tag{11}$$

where

$$d = \sqrt{[\bar{t}(L, \lambda, H) \cdot \hat{u}_1(L_s, \lambda_s)]^2 + [\bar{t}(L, \lambda, H) \cdot \hat{u}_2(L_s, \lambda_s)]^2} \tag{12}$$

is the magnitude of the projection of $\bar{t}(L, \lambda, H)$.

Theoretically, it is possible to determine target latitude and longitude from slant range, azimuth, and altitude. For example, one might search through latitude-longitude pairs $(\cdot, \cdot)$ such that

$$|\bar{t}(\cdot, \cdot, H)| = S \tag{13}$$

and pick one satisfying (10) and (11). In many situations, this is not practical, and other simpler, but approximate, procedures are used. More will be said about the details later. The point of interest here is that the objective is to convert the triplet (S, θ, H) into latitude and longitude.

For purposes of display and computational convenience, representation of target position in terms of latitude and longitude as a point on the ellipsoid is not appealing. Representation of position as a point on some flat surface is better. The latter can be accomplished via a one-to-one mapping of the reference ellipsoid onto a plane. One such mapping can be obtained from the method of stereographic projection in conjunction with the concept of

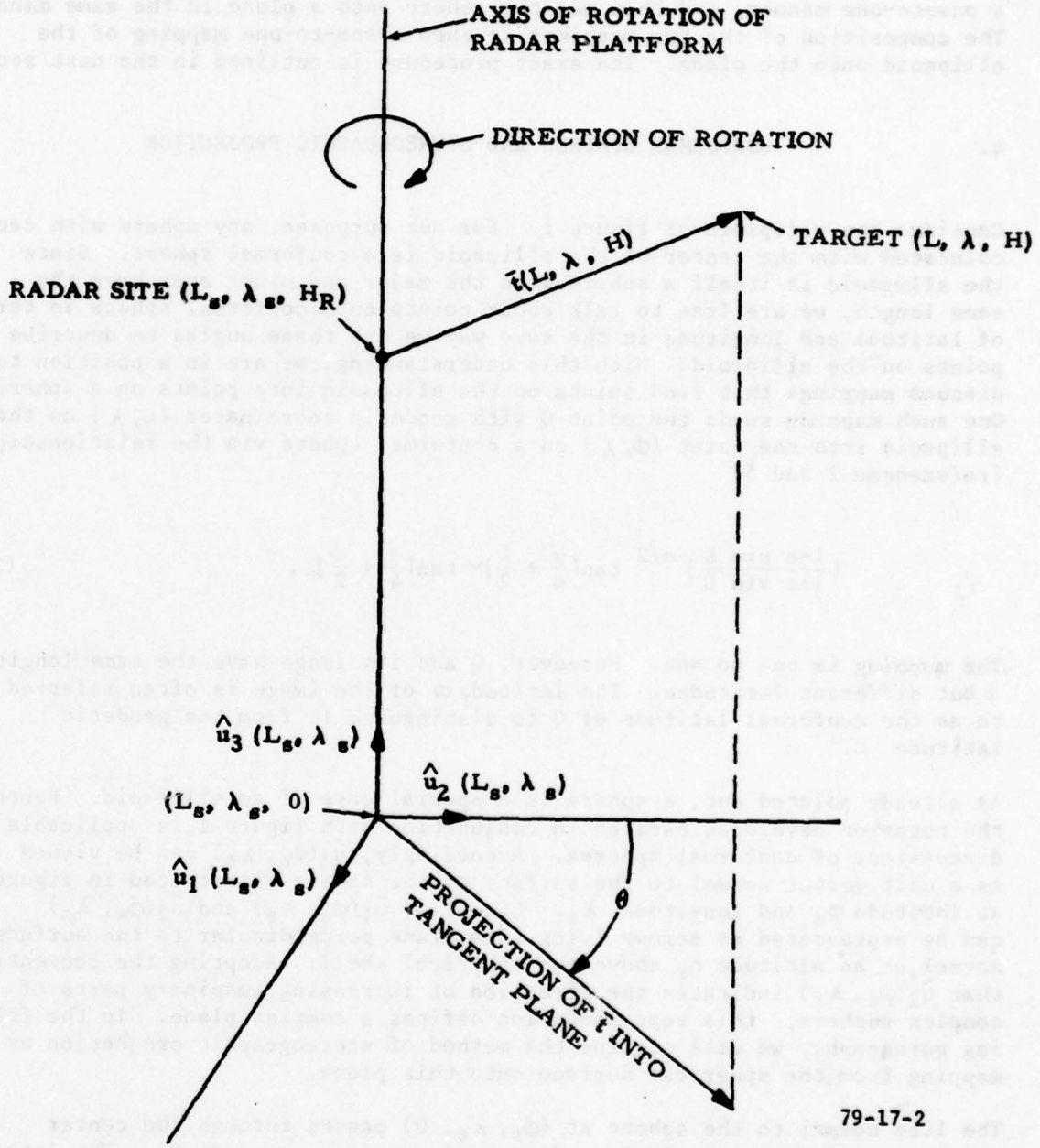

FIGURE 2. SLANT RANGE AND AZIMUTH

conformal spheres. The basic idea is to map the ellipsoid onto a sphere in a one-to-one manner, and then map the sphere onto a plane in the same manner. The composition of the two mappings is then a one-to-one mapping of the ellipsoid onto the plane. The exact procedure is outlined in the next section.

4. CONFORMAL SPHERES AND STEREOGRAPHIC PROJECTION

Consider the ellipsoid of figure 1. For our purposes, any sphere with center colocated with the center of the ellipsoid is a conformal sphere. Since the ellipsoid is itself a sphere when the major and minor axes have the same length, we are free to talk about points on a conformal sphere in terms of latitude and longitude in the same way we use these angles to describe points on the ellipsoid. With this understanding, we are in a position to discuss mappings that send points on the ellipsoid into points on a sphere. One such mapping sends the point Q with geodetic coordinates (L, λ) on the ellipsoid into the point (ϕ, λ) on a conformal sphere via the relationship (references 2 and 5)

$$\left[\frac{1-e \sin L}{1+e \sin L}\right]^{e/2} \tan\left[\frac{\pi}{4} + \frac{L}{2}\right] = \tan\left[\frac{\pi}{4} + \frac{\phi}{2}\right] . \qquad (14)$$

The mapping is one to one. Moreover, Q and its image have the same longitude λ but different latitudes. The latitude ϕ of the image is often referred to as the conformal latitude of Q to distinguish it from the geodetic latitude L.

As already pointed out, a sphere is a special case of an ellipsoid. Hence, the notation developed earlier in conjunction with figure 1 is applicable to discussions of conformal spheres. Accordingly, $\hat{u}_3(\phi_s, \lambda_s)$ can be viewed as a unit vector normal to the surface of the sphere illustrated in figure 3 at latitude ϕ_s and longitude λ_s. Likewise, $\hat{u}_1(\phi_s, \lambda_s)$ and $\hat{u}_2(\phi_s, \lambda_s)$ can be represented as arrows lying in a plane perpendicular to the surface normal at an altitude h_r above the spherical shell. Adopting the convention that $\hat{u}_2(\phi_s, \lambda_s)$ indicates the direction of increasing imaginary parts of complex numbers, this representation defines a complex plane. In the following paragraphs, we will outline the method of stereographic projection as a mapping from the spherical surface onto this plane.

The line normal to the sphere at $(\phi_s, \lambda_s, 0)$ passes through the center and intersects the spherical surface again at $(-\phi_s, \lambda_s + \pi, 0)$. The latter is the focal point for stereographic projection. Under the projection mapping, the image of a point A on the spherical shell is just the point I where the plane intersects the line through A and the focal point.

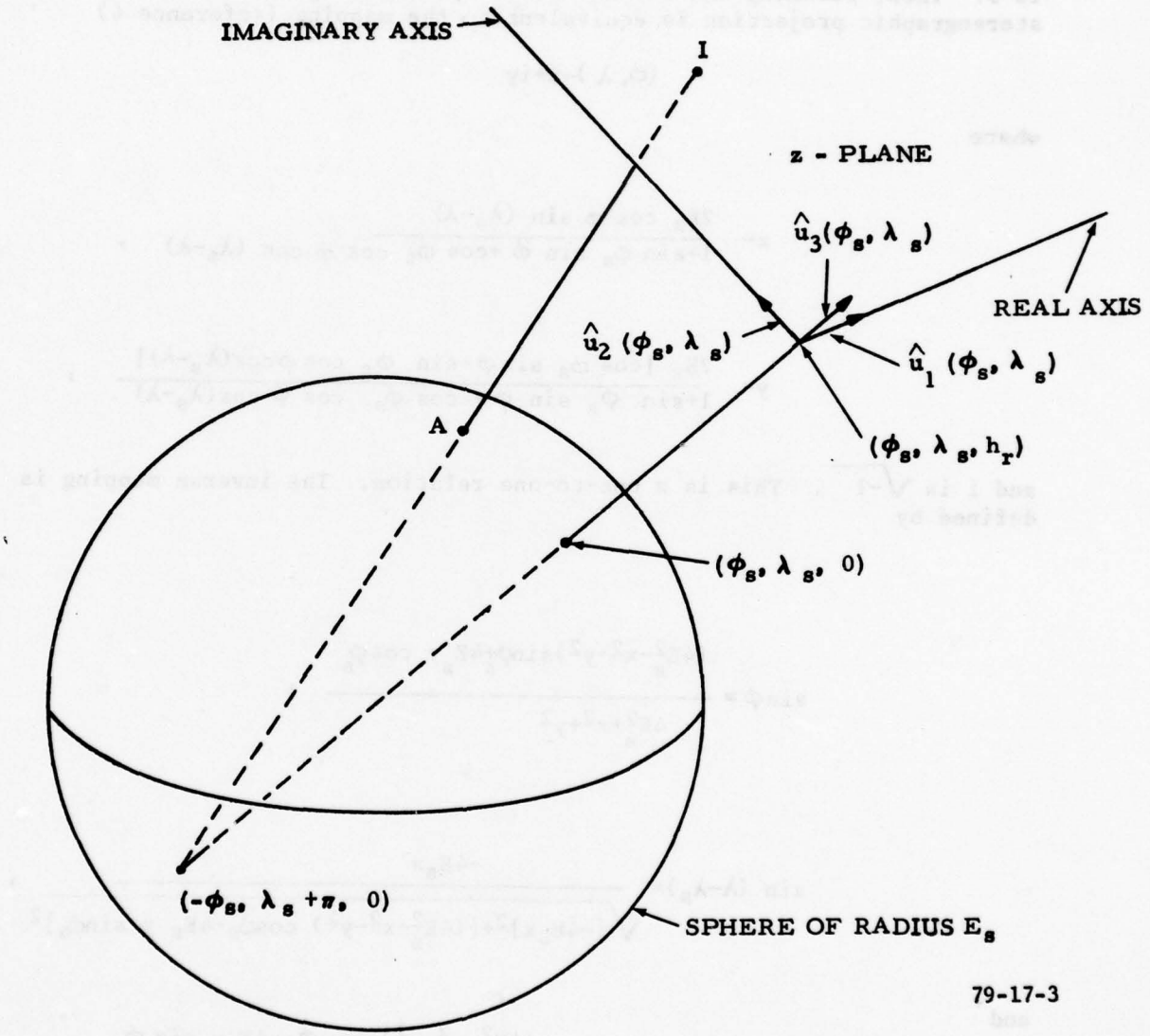

FIGURE 3. STEREOGRAPHIC PROJECTION

Suppose ϕ is the latitude and λ the longitude of A, and x and y represent the real and imaginary parts of the complex representation of I. Also, for the moment, suppose that the projection plane is tangent to the sphere; i.e., h_r is 0. Then, assuming the radius of the sphere is E_s, it can be shown that stereographic projection is equivalent to the mapping (reference 4)

$$(\phi, \lambda) \rightarrow x+iy \tag{15}$$

where

$$x = \frac{2E_s \cos\phi \sin(\lambda_s-\lambda)}{1+\sin\phi_s \sin\phi + \cos\phi_s \cos\phi \cos(\lambda_s-\lambda)}, \tag{16}$$

$$y = \frac{2E_s [\cos\phi_s \sin\phi - \sin\phi_s \cos\phi \cos(\lambda_s-\lambda)]}{1+\sin\phi_s \sin\phi + \cos\phi_s \cos\phi \cos(\lambda_s-\lambda)}, \tag{17}$$

and i is $\sqrt{-1}$. This is a one-to-one relation. The inverse mapping is defined by

$$\sin\phi = \frac{(4E_s^2-x^2-y^2)\sin\phi_s + 4E_s y \cos\phi_s}{4E_s^2+x^2+y^2}, \tag{18}$$

$$\sin(\lambda-\lambda_s) = \frac{-4E_s x}{\sqrt{[-4E_s x]^2+[(4E_s^2-x^2-y^2)\cos\phi_s - 4E_s y \sin\phi_s]^2}}, \tag{19}$$

and

$$\cos(\lambda-\lambda_s) = \frac{(4E_s^2-x^2-y^2)\cos\phi_s - 4E_s y \sin\phi_s}{\sqrt{[-4E_s x]^2+[(4E_s^2-x^2-y^2)\cos\phi_s - 4E_s y \sin\phi_s]^2}}. \tag{20}$$

The preceding equations characterize stereographic projection in the case where the projection plane is tangent to the sphere. Assume now that it is elevated at altitude h_r. Then the image of A is just a scalar multiple of the complex number that is obtained when the altitude vanishes. The multiplicative factor is

$$\frac{1+h_r}{2E_s} . \tag{21}$$

In the case of the inverse procedure, this factor is divided into the complex number obtained from the elevated plane, and then the equations (18)-(20) are applied to the result.

We now return to the case where the projection plane altitude h_r is 0. Let us refer to the complex plane tangent to the conformal sphere of radius E_s at latitude ϕ_s and longitude λ_s as the z-plane. In addition, let us consider another conformal sphere of radius E_r and a complex plane tangent to it at latitude ϕ_r and longitude λ_r. We will call the latter plane the w-plane. It has been shown that the mapping defined by (15)-(17) stereographically projects longitude and conformal latitude into the z-plane. Likewise, by making the obvious substitutions, the same equations can be used to map longitude and conformal latitude into the w-plane. Since both mappings are one-to-one, an obvious composition of the second and the inverse of the first defines a one-to-one mapping of the z-plane onto the w-plane. Under this mapping and subject to the condition that

$$|\lambda_r - \lambda_s| < 90^\circ, \tag{22}$$

it can be shown that the image w of an element z is given by the formula (reference 4)

$$w = \frac{\frac{E_r}{E_s} z \varepsilon^{-i\beta} + w_o}{1 - \frac{z \varepsilon^{-i\beta} w_o^*}{4E_r E_s}} \tag{23}$$

where w_o^* is the conjugate of w_o, $|\beta|$ does not exceed 90°, and

$$\tan \beta = - \frac{\sin(\lambda_r-\lambda_s)\ (\sin\phi_r+\sin\phi_s)}{(1+\sin\phi_r \sin\phi_s)\cos(\lambda_r-\lambda_s)+\cos\phi_r\cos\phi_s} . \tag{24}$$

Obviously, the complex number w_o is just the image of the origin of the z-plane. However, it is clear from the definition of the mapping that any element of the z-plane and its image represent the same longitude and latitude. Consequently, the real and imaginary parts of w_o can be found from (16) and (17) by replacing the subscript s with r. As will be seen shortly, the constraint (22) is not difficult to meet in many practical situations.

Equation (23) is important in some applications where measurements taken from a multitude of far-flung radars are used for surveillance purposes at a single site. As will be seen in the following section, estimates of longitude and conformal latitude from measurements of slant range and azimuth by a single radar in conjunction with reports of target altitude can be formed by means of a mapping into a complex plane tangent to an appropriate sphere at the longitude and conformal latitude of the radar site. This plane corresponds to the z-plane, and there are as many such complex planes as there are radars. Each of these is mapped into a single master plane, corresponding to the w-plane, via a functional relationship analogous to (23). Thus, images on the master plane represent longitudes and conformal latitudes of targets within the composite of the coverage regions of many individual radars. Clearly, the constraint (22) will be satisfied so long as the absolute difference between the longitudes of points of tangency of the master plane and the local radar plane does not exceed 90° for every radar.

5. CONVERSION

In this section, we consider a radar at longitude λ_s, geodetic latitude L_s, and altitude H_R relative to the reference ellipsoid. We also consider a target at altitude H for which the slant range and azimuth relative to the radar are S and θ, respectively. As pointed out earlier, target latitude and longitude can be determined from S, θ, and H. Here, we review how this is accomplished in some practical situations by means of an approximation based upon the method of stereographic projection and the assumption of a spherical earth.

In the vicinity of the radar, the surface of the reference ellipsoid is somewhat like that of a sphere of radius

$$E_s = |\bar{s}(L_s, \lambda_s)| , \tag{25}$$

the distance between the center of the ellipsoid and the orthogonal projection of the radar site onto the ellipsoidal surface. The geometry is illustrated in figure 4 where the radar is pictured as a point removed a radial distance H_R from the spherical shell. This configuration is used to develop equations employed in radar systems for converting slant range, azimuth, and altitude into latitude and longitude or the equivalent thereof.

Consistent with the spherical geometry of figure 4, the orthogonal projection of the target T onto the geoid is represented by the intersection A of the

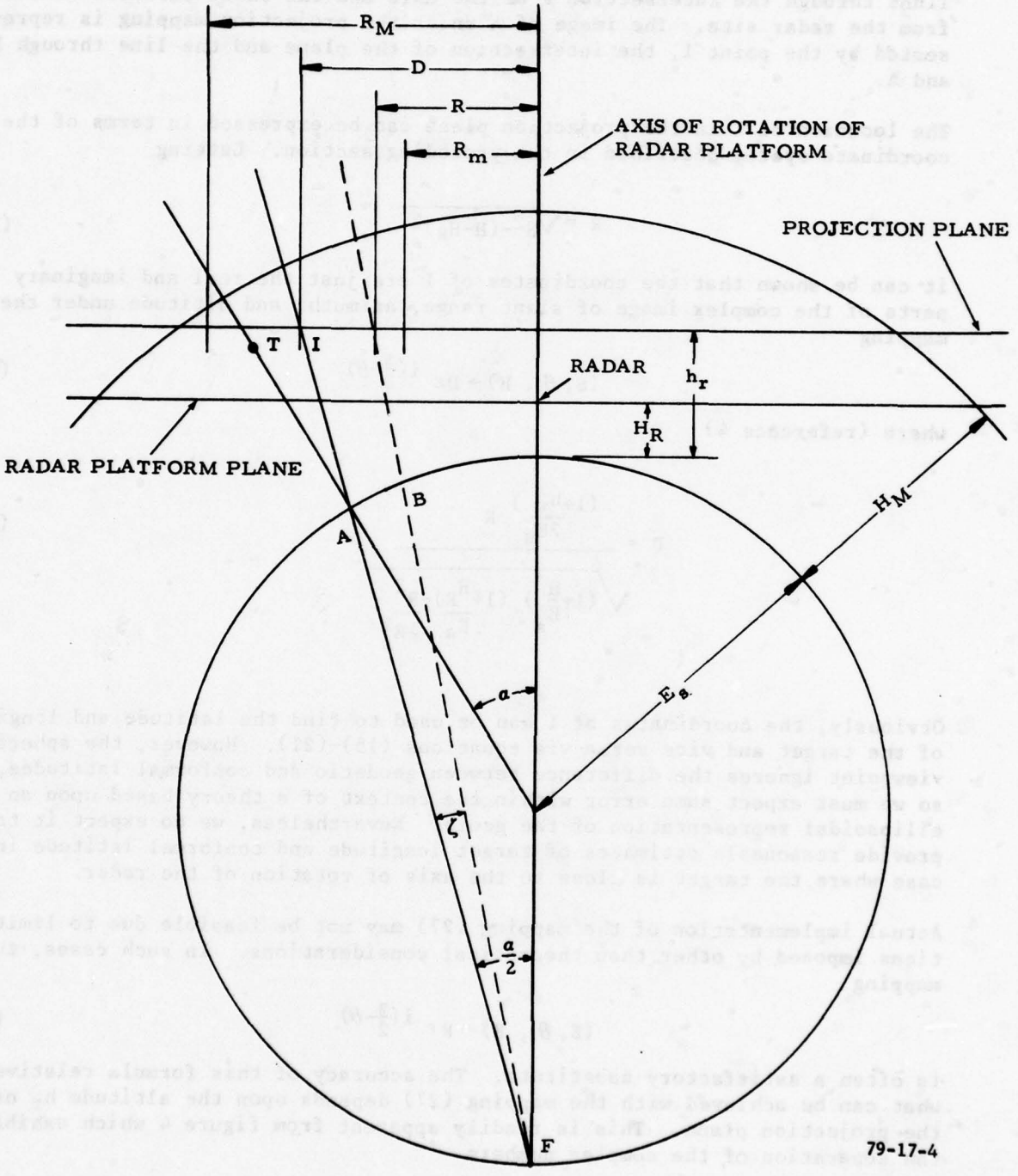

FIGURE 4. SPHERICAL EARTH CONVERSION GEOMETRY

spherical shell and the radial line passing through the target. Points on the shell are stereographically projected into a plane perpendicular to the axis of rotation of the radar platform at altitude h_r. This is accomplished by lines through the intersection F of the axis and the shell furthest removed from the radar site. The image of A under the projection mapping is represented by the point I, the intersection of the plane and the line through F and A.

The location of I in the projection plane can be expressed in terms of the coordinate system described in the preceding section. Letting

$$R = \sqrt{S^2-(H-H_R)^2} \quad , \tag{26}$$

it can be shown that the coordinates of I are just the real and imaginary parts of the complex image of slant range, azimuth, and altitude under the mapping

$$(S, \theta , H) \rightarrow D\varepsilon^{\,i(\frac{\pi}{2}-\theta)} \tag{27}$$

where (reference 4)

$$D = \frac{(1+\frac{h_r}{2E_s})\,R}{\sqrt{(1+\frac{H}{E_s})\,(1+\frac{H_R}{E_s})-\frac{R^2}{4E_s^2}}} \quad . \tag{28}$$

Obviously, the coordinates of I can be used to find the latitude and longitude of the target and vice versa via equations (15)-(21). However, the spherical viewpoint ignores the difference between geodetic and conformal latitudes, and so we must expect some error within the context of a theory based upon an ellipsoidal representation of the geoid. Nevertheless, we do expect it to provide reasonable estimates of target longitude and conformal latitude in the case where the target is close to the axis of rotation of the radar.

Actual implementation of the mapping (27) may not be feasible due to limitations imposed by other than theoretical considerations. In such cases, the mapping

$$(S, \theta , H) \rightarrow R\varepsilon^{\,i(\frac{\pi}{2}-\theta)} \tag{29}$$

is often a satisfactory substitute. The accuracy of this formula relative to what can be achieved with the mapping (27) depends upon the altitude h_r of the projection plane. This is readily apparent from figure 4 which exhibits the separation of the complex numbers

$$D\varepsilon^{i(\frac{\pi}{2}-\theta)} \text{ and } R\varepsilon^{i(\frac{\pi}{2}-\theta)} \tag{30}$$

in the plane as well as the relative position of the corresponding images A and B on the spherical surface under the projection mapping. Happily, if we accept the existence of some maximum altitude H_M for targets of interest, then it is possible to find a projection plane altitude that is optimal in a minimax sense.

In particular, referring to figure 4, it can be shown that R increases monotonically from a minimum value R_m to a maximum value R_M as the target T moves outward along a radial line from the radar platform plane to the maximum altitude H_M. These extreme values of R are functions of the angle α between the radial line through the target and the axis of rotation of the radar. When

$$\cos\alpha = \left(1 + \frac{H_R}{E_s}\right)^{\frac{2}{3}} \left(1 + \frac{H_M + H_R}{E_s} + \frac{H_M H_R}{E_s^2}\right)^{-\frac{1}{3}}, \tag{31}$$

the difference

$$R_M - R_m \tag{32}$$

is maximal (reference 4). From figure 4, we expect that there exists a projection plane altitude for which the image I of a target on the maximizing radial splits the difference into equal parts. Indeed, this is the case, and the corresponding altitude is (reference 4)

$$h_r = 2E_s\left\{\left[\tfrac{1}{2}\left(1+\frac{H_R+H_M+H_RH_M}{E_s}\right)\frac{1}{E_s^2}\right]^{\frac{1}{3}} + \tfrac{1}{2}\left(1+\frac{H_R}{E_s}\right)^{\frac{2}{3}}\right]^{\frac{3}{2}} - 1\right\}. \tag{33}$$

In fact, for any given projection plane, $|D-R|$ assumes a maximum over all target positions below altitude H_M and above the radar platform plane, and it can be shown that the maximum is least when the projection plane altitude is given by (33).

The observations of the preceding paragraphs can be used to show that the altitude (33) is near optimal in another sense. Consider the angle ζ in figure 4 between the lines that intersect in the stereographic projection center F and cut the complex plane at the points represented by the numbers (30). At a give projection plane altitude, this angle assumes a maximum value over the target positions below altitude H_M and above the radar platfrom plane. On the other hand, the angle of the radial for which the difference between R_m and R_M is maximal is small when the right side of (31) is close to 1. In cases such as this, it is not difficult to argue that the maximum value of ζ is essentially minimized by the projection plane at the altitude (33).

6. CONVERSION ERRORS - DEFINITIONS

Consider a target at altitude H, longitude λ, and geodetic latitude L relative to the reference ellipsoid. Let S and θ be the slant range and azimuth, respectively, of the target relative to the radar described in the previous section at altitude H_R, longitude λ_s, and geodetic latitude L_s. Also, let us agree to use "z-plane" to denote the complex plane tangent to the conformal sphere of radius E_s, defined by (25), at the longitude and conformal latitude ϕ_s of the radar. Finally, suppose the conversion process is accomplished by mapping (S, θ, H) into the point

$$z_c=\left[1+\frac{h_r}{2E_s}\right]^{-1} R\,\epsilon^{\,i(\frac{\pi}{2}-\theta)} \tag{34}$$

of the z-plane where R is defined by (26).

Let ϕ represent the conformal latitude of the target and

$$z=x+iy \tag{35}$$

be the z-plane image of the point (ϕ, λ) on the conformal sphere under the mapping (15). From (14)-(17), it is clear that the relation

$$(L, \lambda)\rightarrow z \tag{36}$$

defines a one-to-one mapping M from the ellipsoid onto the z-plane. The mapping is essentially a transformation of geodetic latitude into conformal latitude followed by stereographic projection of the conformal sphere onto the z-plane. Obviously,

$$M(L_s, \lambda_s)=0, \tag{37}$$

since the longitude and geodetic latitude of the radar site must map into the origin of the z-plane.

Since M is one-to-one, the point z uniquely determines target longitude and geodetic latitude. Moreover, these angles together with target altitude can be used to find target slant range and azimuth via (8)-(12). Finally, the image z_c of the target in the z-plane under the conversion process (34) is determined by target altitude, slant range, and azimuth. Thus, for a given radar configuration defined in terms of maximum target altitude H_M and the geodetic coordinates of the site itself, z_c can be viewed as a function of target altitude and the image z of the target in the z-plane under the mapping M. Indeed, this is the viewpoint that is adopted in the following paragraphs.

Ideally, the objective of conversion is to map (S, θ, H) into z. However, due to geometric and analytical approximations, the complex numbers z and z_c are not necessarily the same. The difference

$$\delta_1(z,H)=|z-z_c| \ , \tag{38}$$

for want of a better name, will be called the conversion error. As indicated in figure 5, it is also convenient to talk about the errors

$$\delta_2(z,H)=|z|-|z_c| \tag{39}$$

and

$$\delta_3(z,H)=\arg(z)-\arg(z_c) \tag{40}$$

where "arg" denotes the argument of a complex number.

We will have occasion to use the polar forms of the z-plane images of the target under the mapping M and the conversion process, namely

$$z=\rho\varepsilon^{i\gamma} \qquad \text{and} \qquad z_c=\rho_c\varepsilon^{i\gamma_c} \tag{41}$$

We will call ρ and γ the range and angle of the target, whereas ρ_c and γ_c will be referred to as the range and angle due to conversion. Thus, (39) and (40) can be viewed as errors in range and angle that together give rise to the overall coversion error (38). In what follows, we will often abuse the notation introduced in (38)-(40) by deferring to the polar form of complex numbers and writing $\delta_k(\rho, \gamma, H)$ in place of $\delta_k(z, H)$ for k=1, 2, or 3.

Let us now consider the situation in which target altitude remains constant and the trajectory induced by target motion in the z-plane under the mapping M is a circle centered at the origin. This is equivalent to holding ρ and H constant while allowing γ to traverse the continuum between 0 and 2π radians. In general, the error $\delta_k(\rho, \gamma, H)$ will oscillate about the median

$$m_k(\rho,H)=\left[\max_{0<\gamma\leq 2\pi}\delta_k(\rho,\gamma,H)+\min_{0<\gamma\leq 2\pi}\delta_k(\rho,\gamma,H)\right]/2 \tag{42}$$

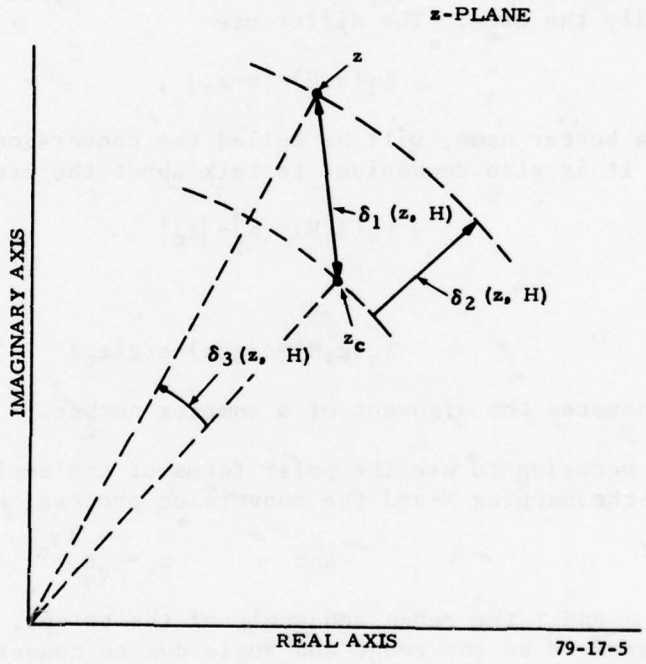

FIGURE 5. CONVERSION ERROR

with an amplitude[1]

$$a_k(\rho,H)=\max_{0<\gamma\leq 2\pi} \delta_k(\rho,\gamma,H)-m_k(\rho,H) \quad . \tag{43}$$

For example, figure 6 illustrates the behavior of the range and angle errors when target altitude is 40,000 feet, the target range is 160 nautical miles (1 nautical mile = 1,852 meters) and h_r satisfies (33). As shown, the median range error is .0047 nautical mile accompanied by an amplitude of .012 nautical mile.

7. CONVERSION ERRORS - NUMERICAL RESULTS

In this section, we will consider some numerical results obtained for conversion errors in connection with radar site locations in the Northern Hemisphere on parallels 28, 38, and 48 at altitudes of 0 and 10,000 feet. In each case, the maximum altitude H_M for targets of interest is 60,000 feet. Also, the elevation of the projection plane is given by the right side of (33), and so it tends to minimize the maximum conversion error over targets above the radar platform plane and below H_M. However, it is well to recognize that little is to be gained by examining errors associated with targets that are hidden from the field of view of the radar. Thus, rather than proceeding directly with a discussion of errors, something will be said first about what we mean by radar horizon.

Actual radars are capable of detecting targets somewhat below the line-of-sight horizon. Nevertheless, it is an obvious consequence of the mathematical setup used in this paper that a necessary condition for a target to be visible to the radar is that the line segment connecting the two entities does not intersect the reference ellipsoid in more than one point. More specifically, consider the plane defined by the axis of rotation of the radar platform and a line through the radar tangent to the ellipsoid. The line consists of two semi-infinite segments terminating in the point of tangency. One of these contains the radar site. As shown in figure 7, targets in the shaded region of the plane below the other segment and above the surface of the ellipsoid cannot be seen from the radar site.

The collection of semi-infinite line segments that are tangent to the ellipsoid and emanate from the radar site form a cone-like surface. We will refer to the locus of points at which it intersects the ellipsoid as the radar horizon contour. The contour divides the cone into a surface of infinite extent and one of finite extent. We will refer to the union of the surface of infinite extent with the orthogonal projection of the surface of finite extent onto the ellipsoid as the radar horizon surface. As indicated in figure 7, a target above the reference ellipsoid can be seen from the radar site only if it is also above the horizon surface.

---

[1] In the case of a spherical earth model the amplitude $a_k(\rho, H)$ vanishes identically for all k.

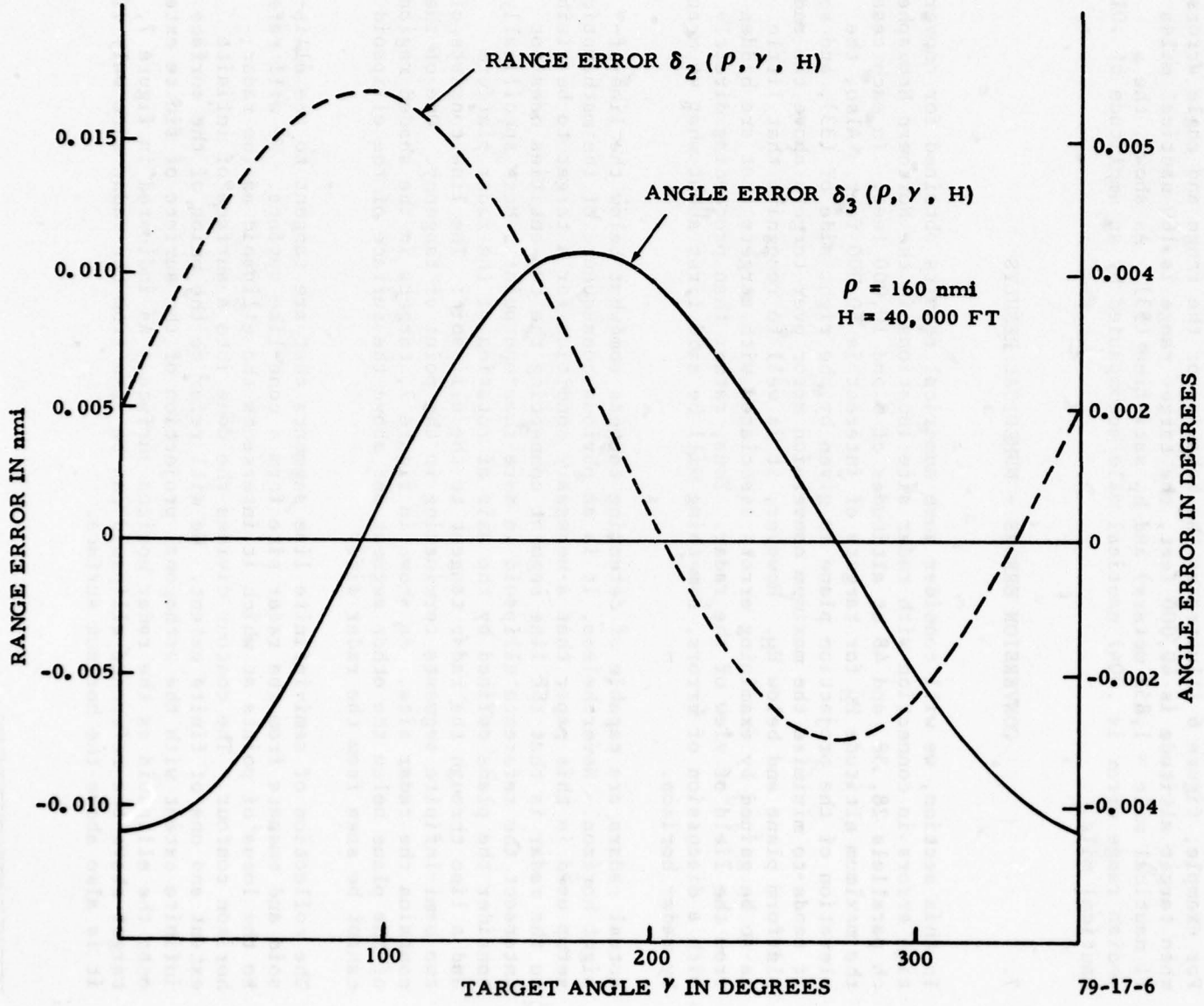

FIGURE 6. RANGE AND ANGLE ERRORS FOR RADAR AT SEA LEVEL ON PARALLEL 38

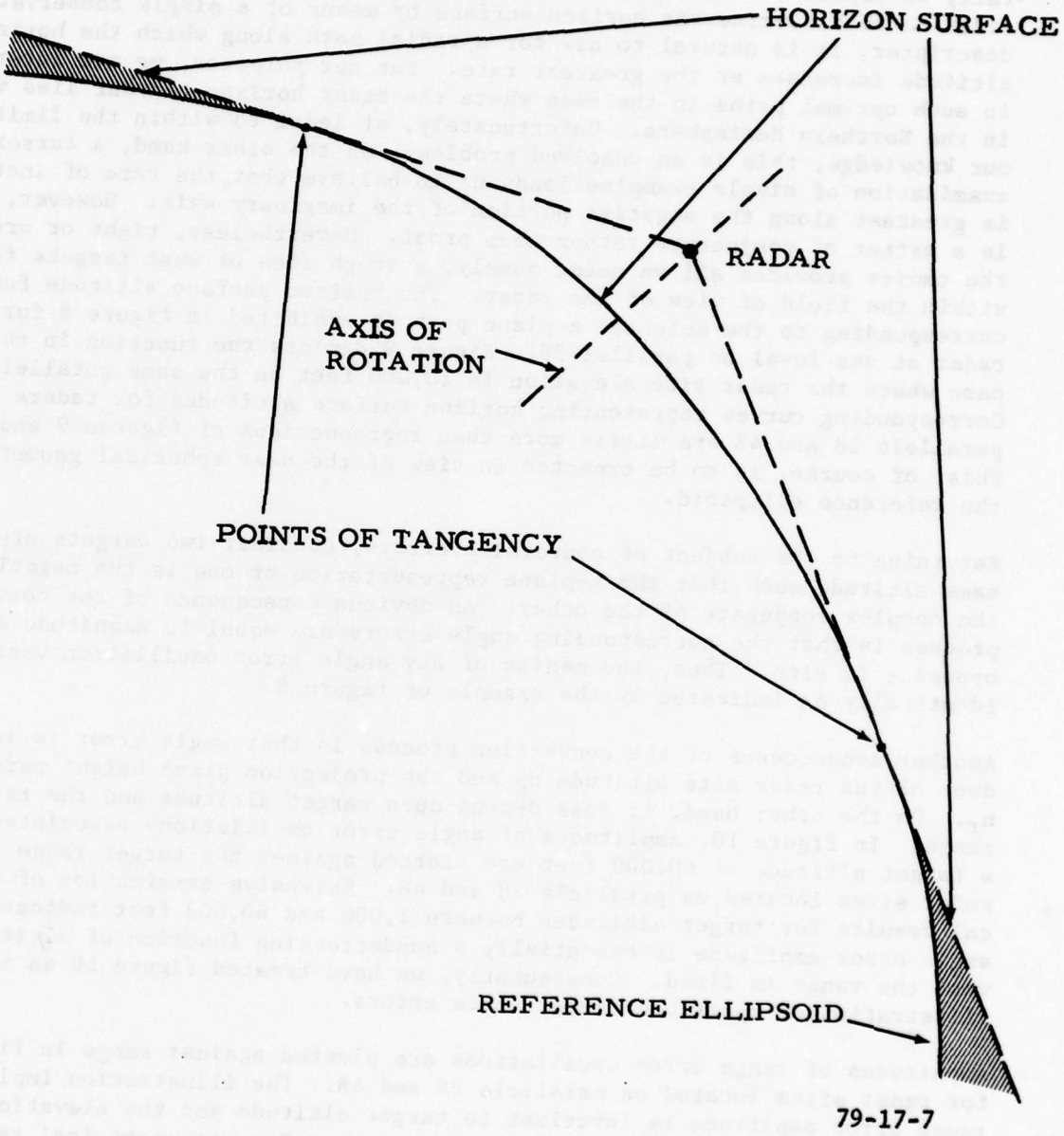

FIGURE 7. RADAR HORIZON

As the point z moves away from the origin of the z-plane along a radial path, we expect the altitude of the horizon surface at the longitude and geodetic latitude represented by $M^{-1}(z)$ to be a non-decreasing function of ρ. In fact, we expect the function to differ for different radial paths. Thus, in order to characterize the horizon surface by means of a single conservative descriptor, it is natural to ask for a radial path along which the horizon altitude increases at the greatest rate. For our purposes, we are interested in such optimal paths in the case where the radar horizon contour lies wholly in the Northern Hemisphere. Unfortunately, at least to within the limits of our knowledge, this is an unsolved problem. On the other hand, a cursory examination of simple examples leads us to believe that the rate of increase is greatest along the negative portion of the imaginary axis. However, this is a matter of conjecture rather than proof. Nevertheless, right or wrong, the choice provides all we need, namely, a rough idea of what targets fall within the field of view of the radar. The horizon surface altitude function corresponding to the selected z-plane path is exhibited in figure 8 for a radar at sea level on parallel 38. Figure 9 depicts the function in the case where the radar site elevation is 10,000 feet on the same parallel. Corresponding curves representing horizon surface altitudes for radars on parallels 28 and 48 are little more than reproductions of figures 9 and 10. This, of course, is to be expected in view of the near spherical geometry of the reference ellipsoid.

Returning to the subject of conversion errors, consider two targets at the same altitude such that the z-plane representation of one is the negative of the complex conjugate of the other. An obvious consequence of the conversion process is that the corresponding angle errors are equal in magnitude and opposite in sign. Thus, the median of any angle error oscillation vanishes identically as indicated by the example of figure 6.

Another consequence of the conversion process is that angle error is independent of the radar site altitude H_R and the projection plane height parameter h_r. On the other hand, it does depend upon target altitude and the target range. In figure 10, amplitudes of angle error oscillations associated with a target altitude of 60,000 feet are plotted against the target range for radar sites located on parallels 28 and 48. Extensive examination of numerical results for target altitudes between 1,000 and 60,000 feet indicates that angle error amplitude is essentially a nondecreasing function of altitude when the range is fixed. Consequently, we have treated figure 10 as an illustration of upper bounds for angle errors.

Amplitudes of range error oscillations are plotted against range in figure 11 for radar sites located on parallels 28 and 48. The illustration implies that range error amplitude is invariant to target altitude and the elevation of the radar site. Strictly speaking, this is not so. However, numerical results obtained for radars at 0 and 10,000 feet and target altitudes between 1,000 and 60,000 feet indicate the variation is less than a few tenths of one meter. For our purposes, such minute differences are irrelevant.

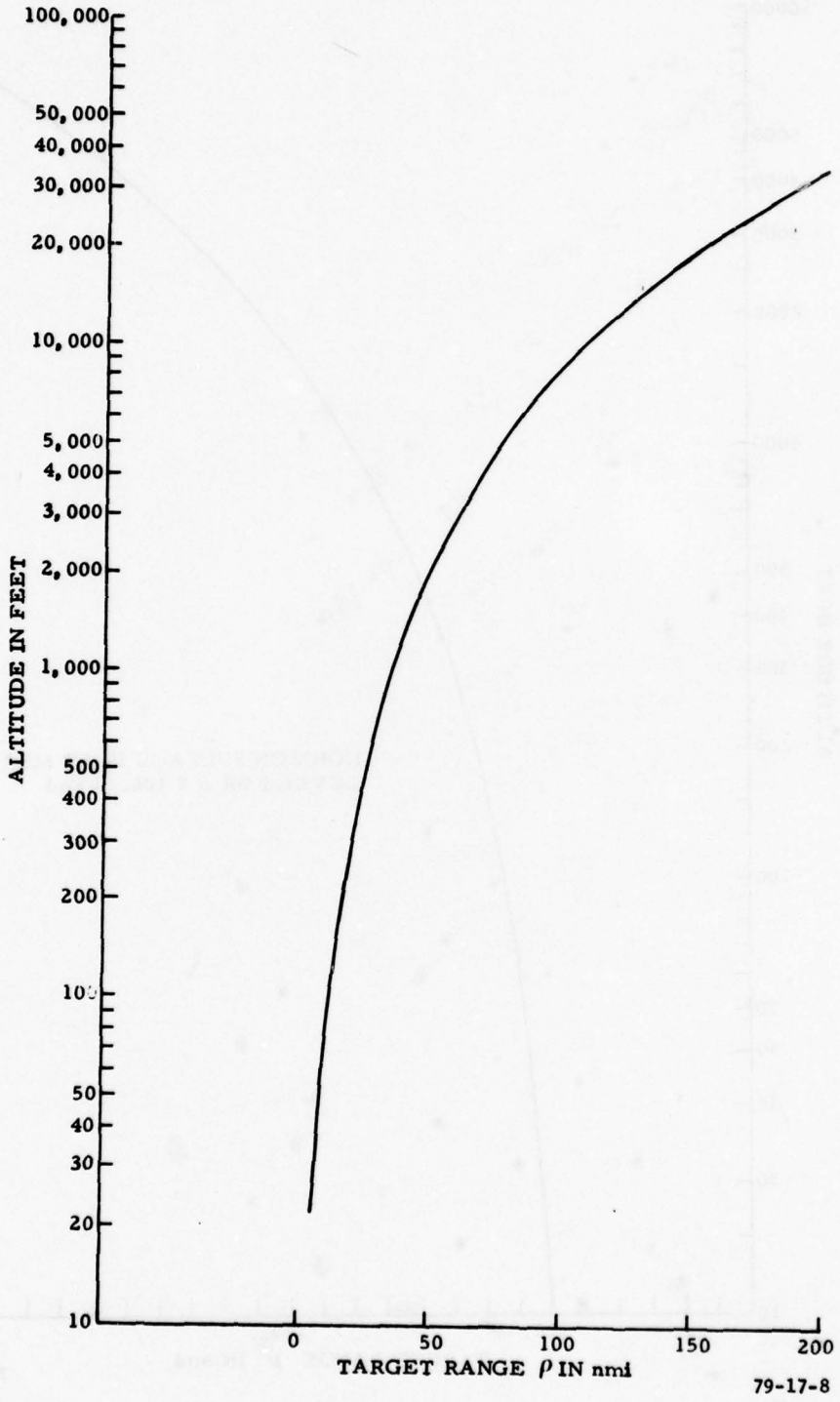

FIGURE 8. ALTITUDE OF HORIZON SURFACE FOR RADAR AT SEA LEVEL ON PARALLEL 38

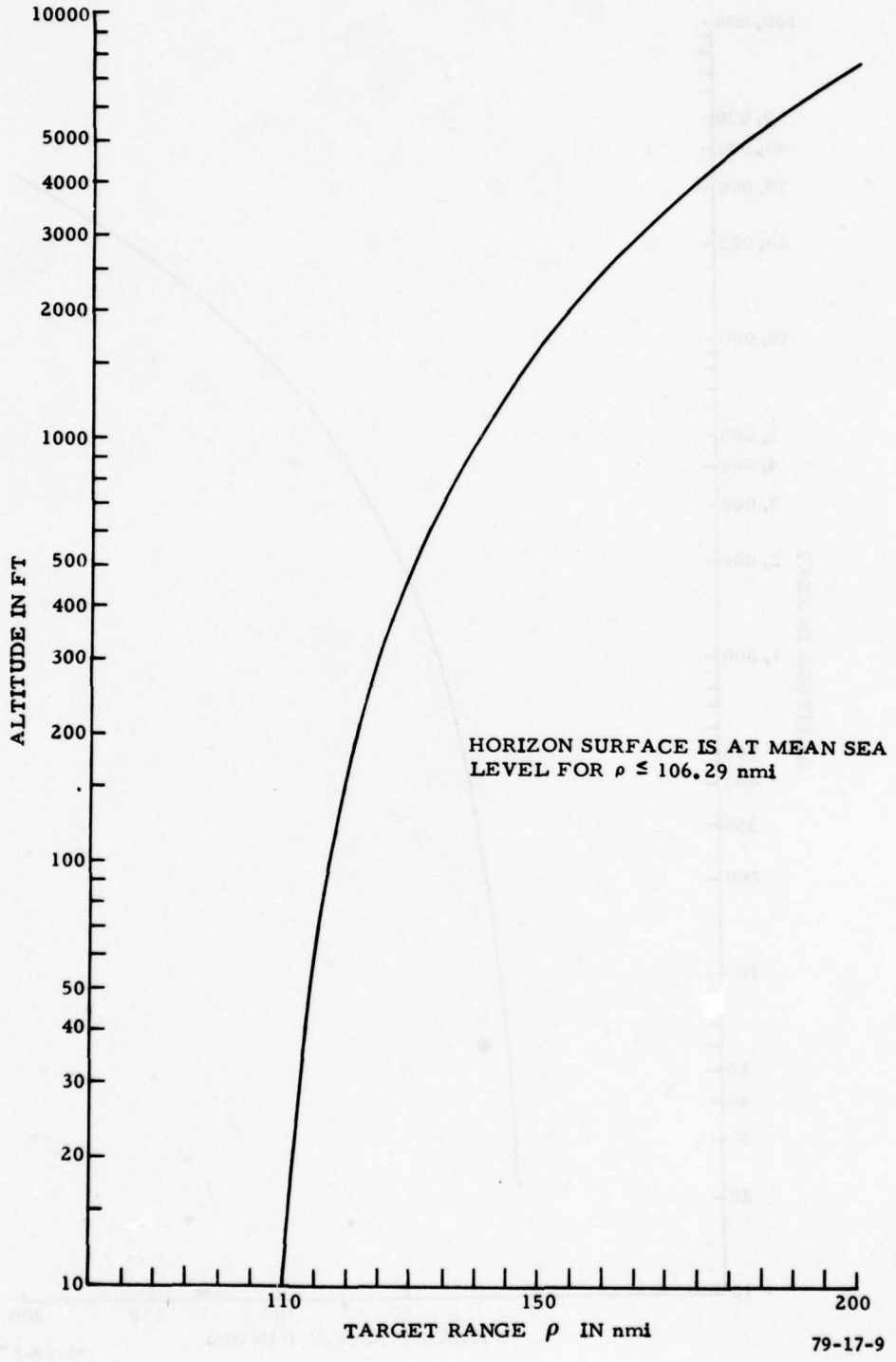

FIGURE 9. ALTITUDE OF HORIZON SURFACE FOR RADAR AT 10,000 FEET ON PARALLEL 38

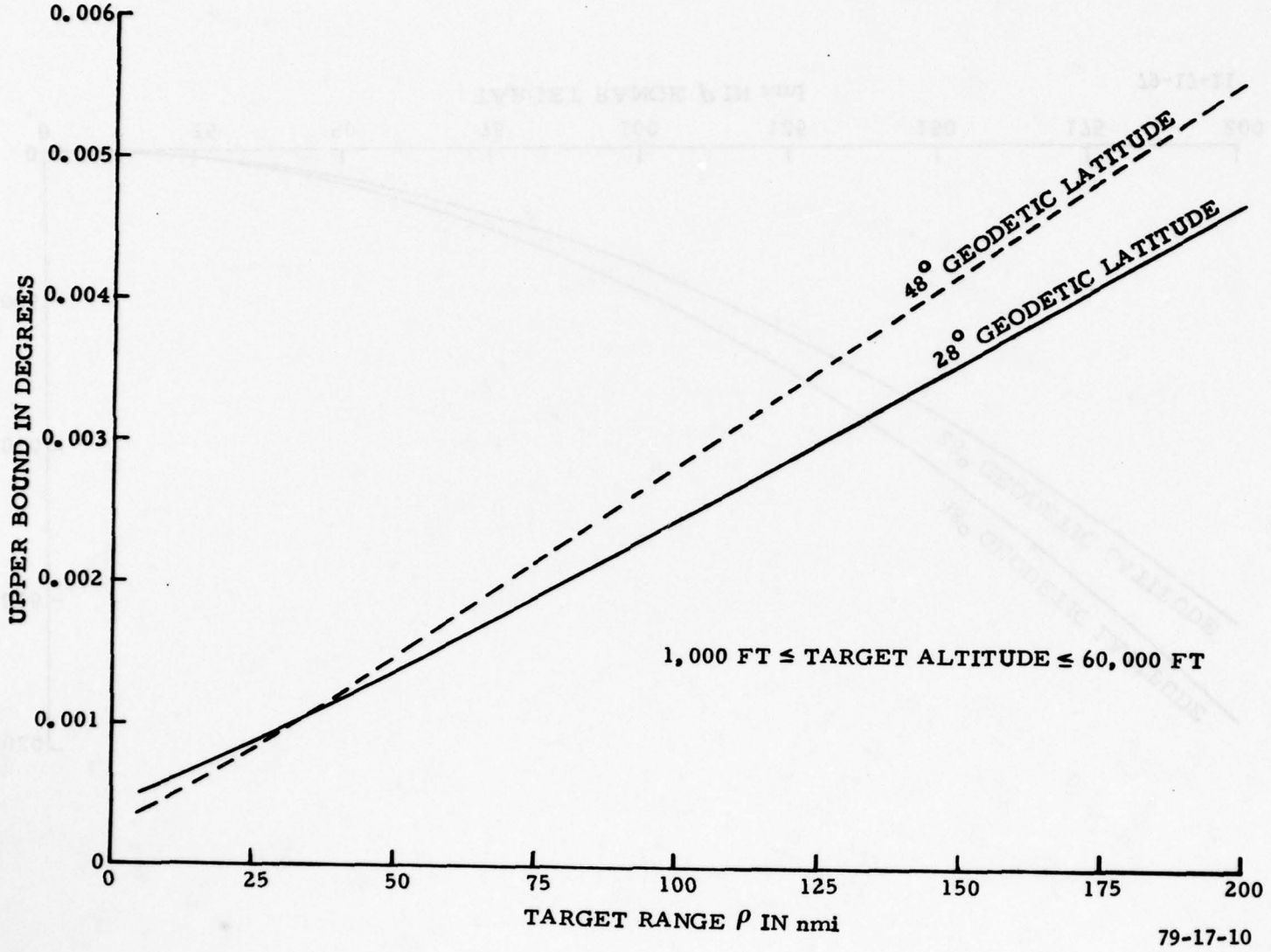

FIGURE 10. UPPER BOUNDS ON ABSOLUTE ANGLE ERROR $|\delta_3(\rho,\gamma,H)|$

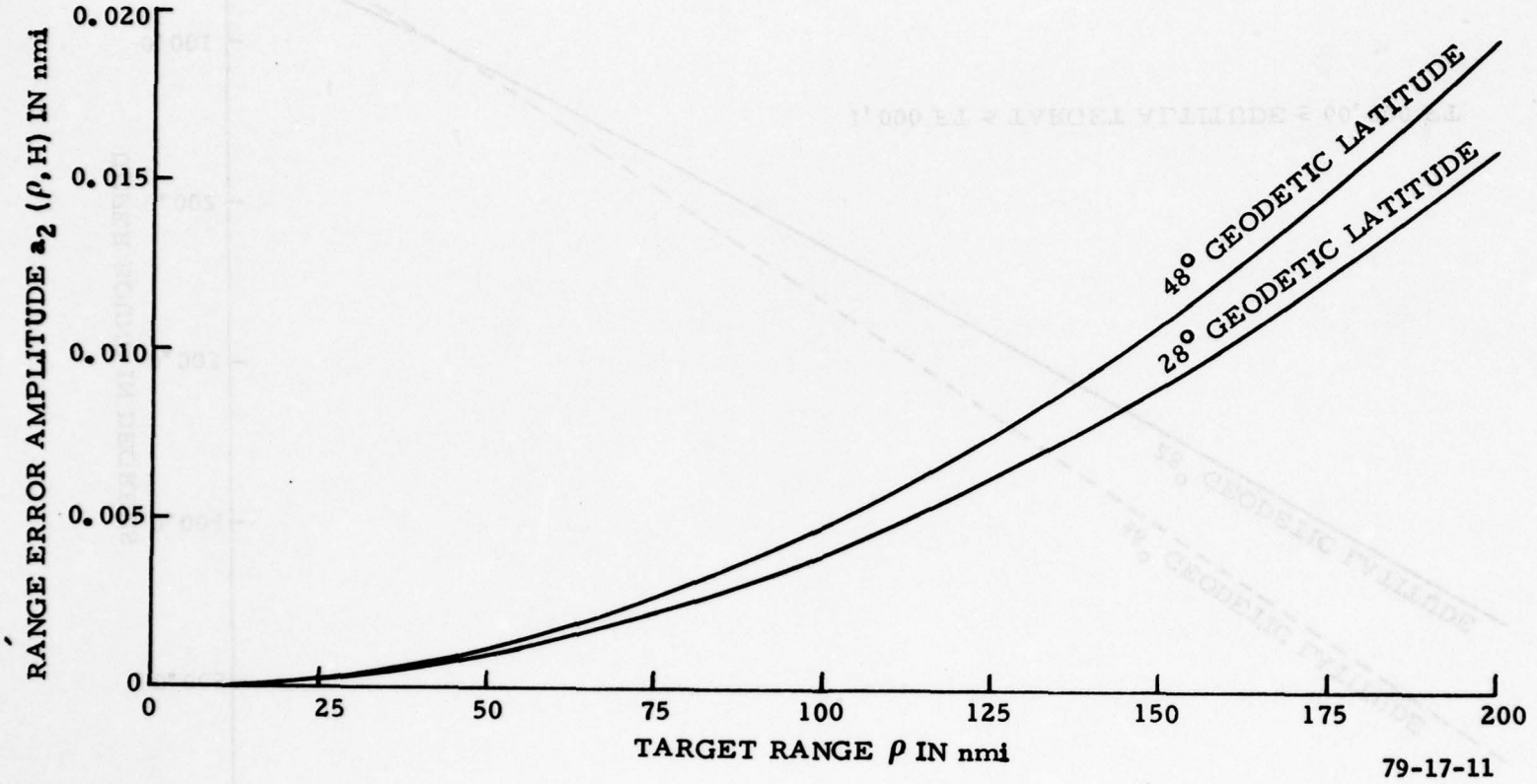

FIGURE 11. RANGE ERROR AMPLITUDE

Figures 12 and 13 illustrate medians of range error oscillations at several different target altitudes for radars at sea level and 10,000 feet. The data were obtained for radar site locations on parallel 38. However, results obtained for parallels 28 and 48 are the same to within .001 nautical mile. Consequently, for our purposes, the illustrations are equally applicable to all three parallels. Actually, this is not surprising. In the case of a spherical earth model, error is invariant to radar site latitude, and we expect this invariance to carry over in some approximate sense to the model embodied in the reference ellipsoid.

Figures 14 and 15 illustrate the maximum overall conversion error for radars on parallel 38. As already pointed out, the projection plane elevation used in this section can be regarded as a solution to a minimax problem involving targets in the region above the radar platform plane and below 60,000 feet. This region corresponds to that portion of figures 14 and 15 below and to the right of the curve associated with targets at 60,000 feet. Thus, the optimality, if any, of the data above and to the left of this boundary is an open question. When figures 14 and 15 are compared with figures 12 and 13, it becomes apparent that median range error contributes heavily to the overall conversion error. In the next section, we will discuss a method for reducing the size of the range error.

8. ALTERNATIVE APPROACHES TO ERROR CONTROL

The surface of the reference ellipsoid in the vicinity of the radar is closely approximated by that of a sphere with radius E_s defined by (25). If, in our mind's eye, we allow the lengths of the semiminor and semimajor axes of the ellipsoid to approach E_s, then angle errors and amplitudes of range error oscillations vanish. All that is left is the median range error $m_2(\rho, H)$. In fact z and z_c of (41) can be obtained by multiplying the complex numbers (30) by the inverse of $1 + h_r/2E_s$. Thus, in the context of a spherical representation of the geoid of radius E_s,

$$m_2(\rho, H) = \rho - R\,[1 + h_r/2E_s]^{-1} \tag{44}$$

where

$$\rho = D\,[1 + h_r/2E_s]^{-1} \tag{45}$$

and R is related to D through the expression (28). From (28) and (45), R can be expressed as a function of ρ, and this can be used to reduce (44) to the form

$$m_2(\rho, H) = \left[1 - \frac{\sqrt{(1 + H/E_s)\,(1 + H_R/E_s)}}{(1 + h_r/2E_s)\,\sqrt{1 + \rho^2/4E_s^2}}\right]\rho \quad . \tag{46}$$

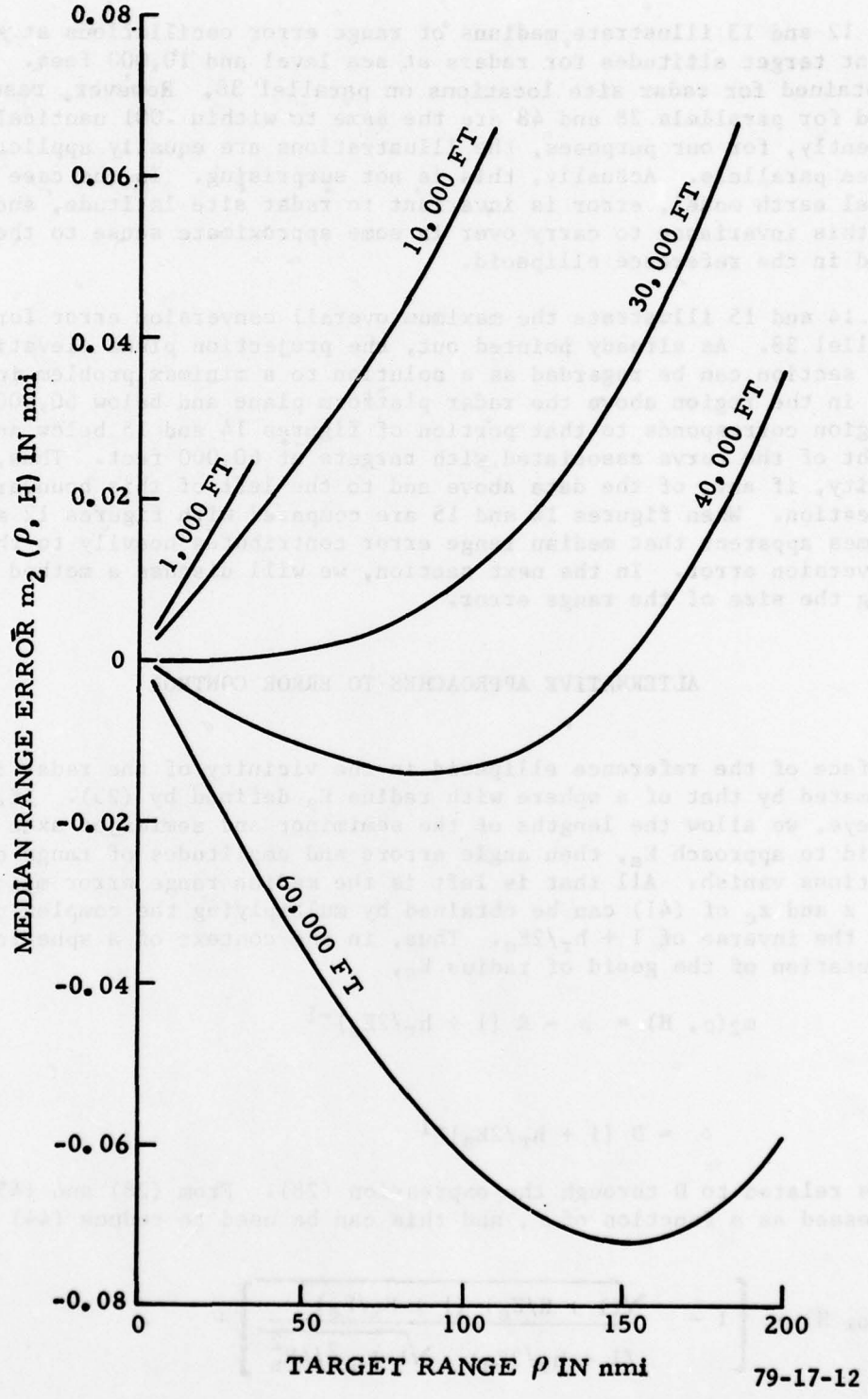

FIGURE 12. MEDIAN RANGE ERROR FOR RADAR AT SEA LEVEL

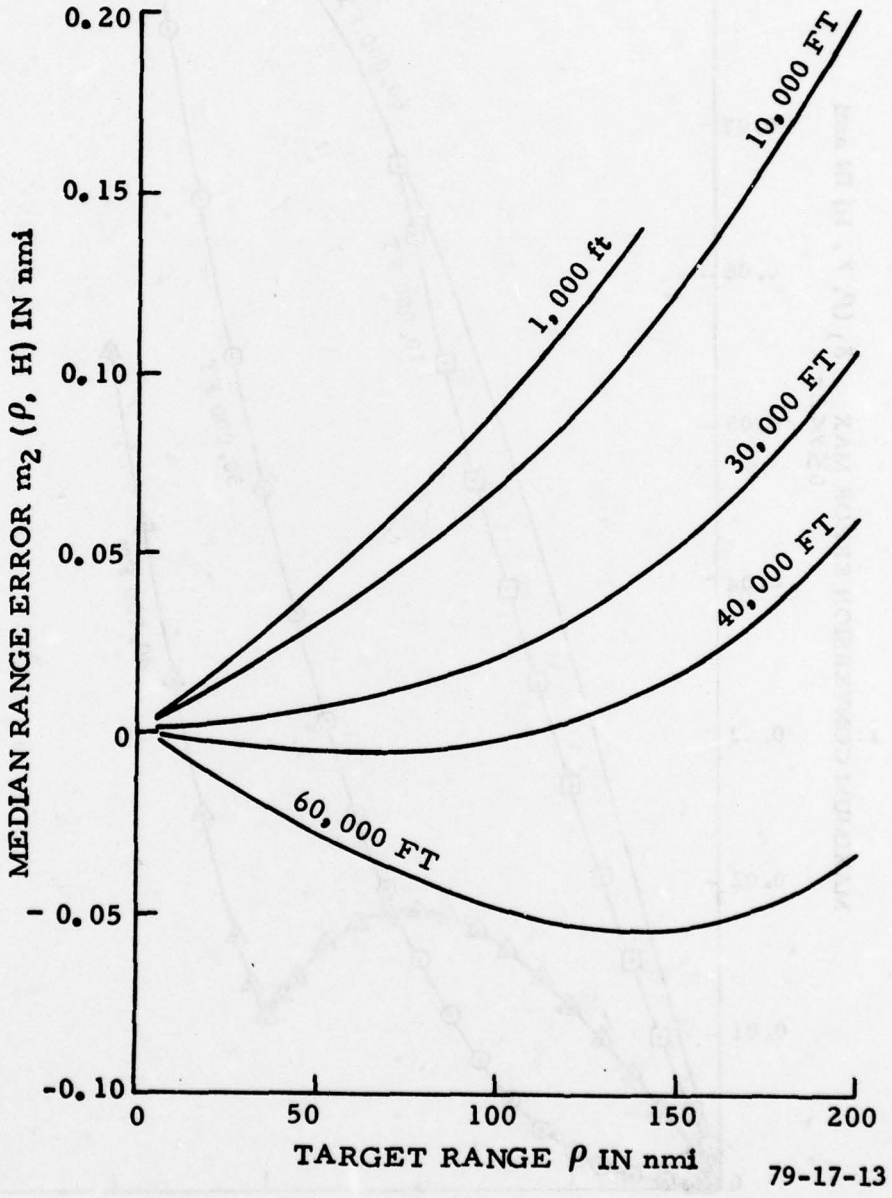

FIGURE 13. MEDIAN RANGE ERROR FOR RADAR AT 10,000 FEET

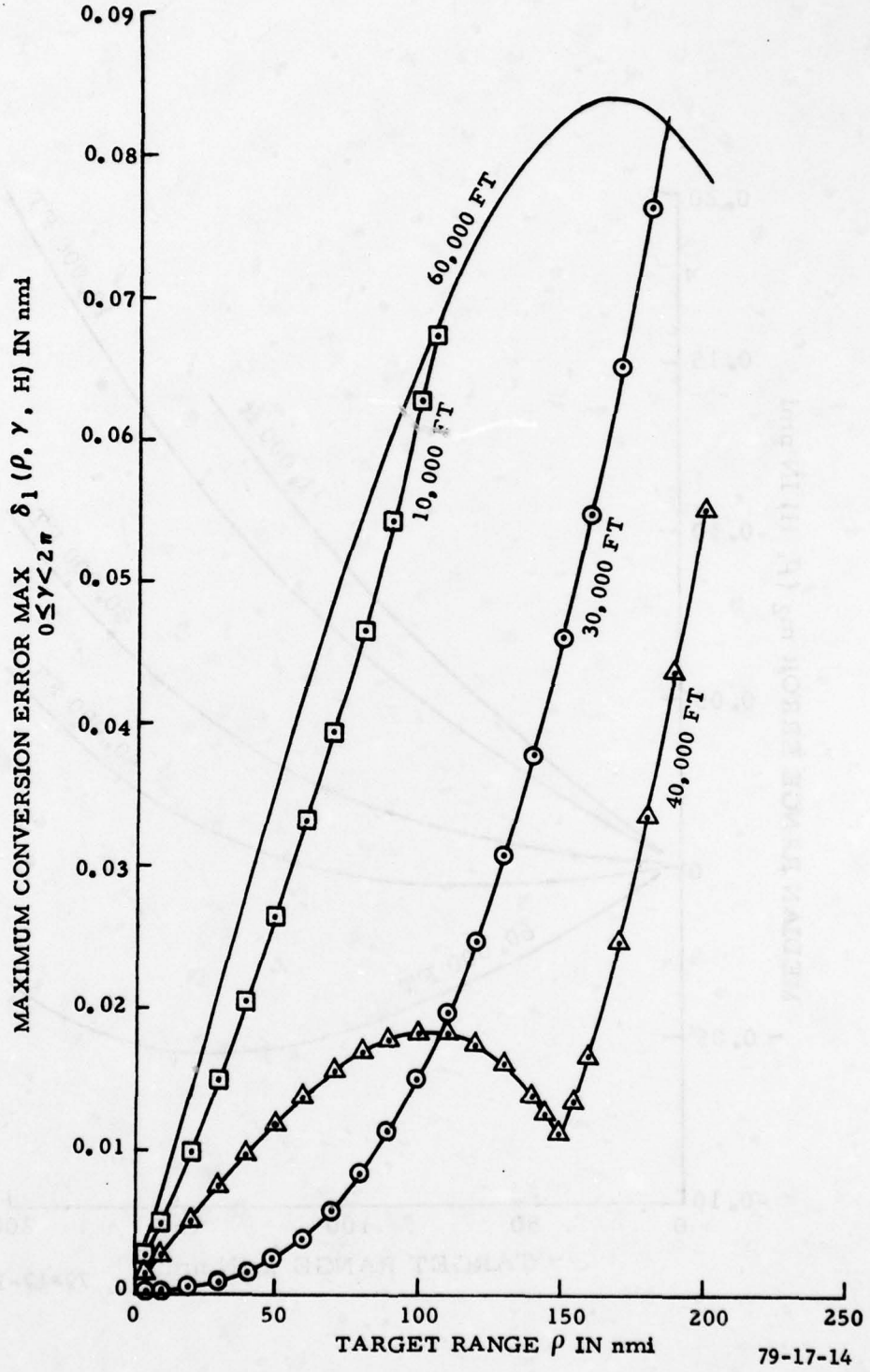

FIGURE 14. MAXIMUM CONVERSION ERROR FOR RADAR AT SEA LEVEL ON PARALLEL 38

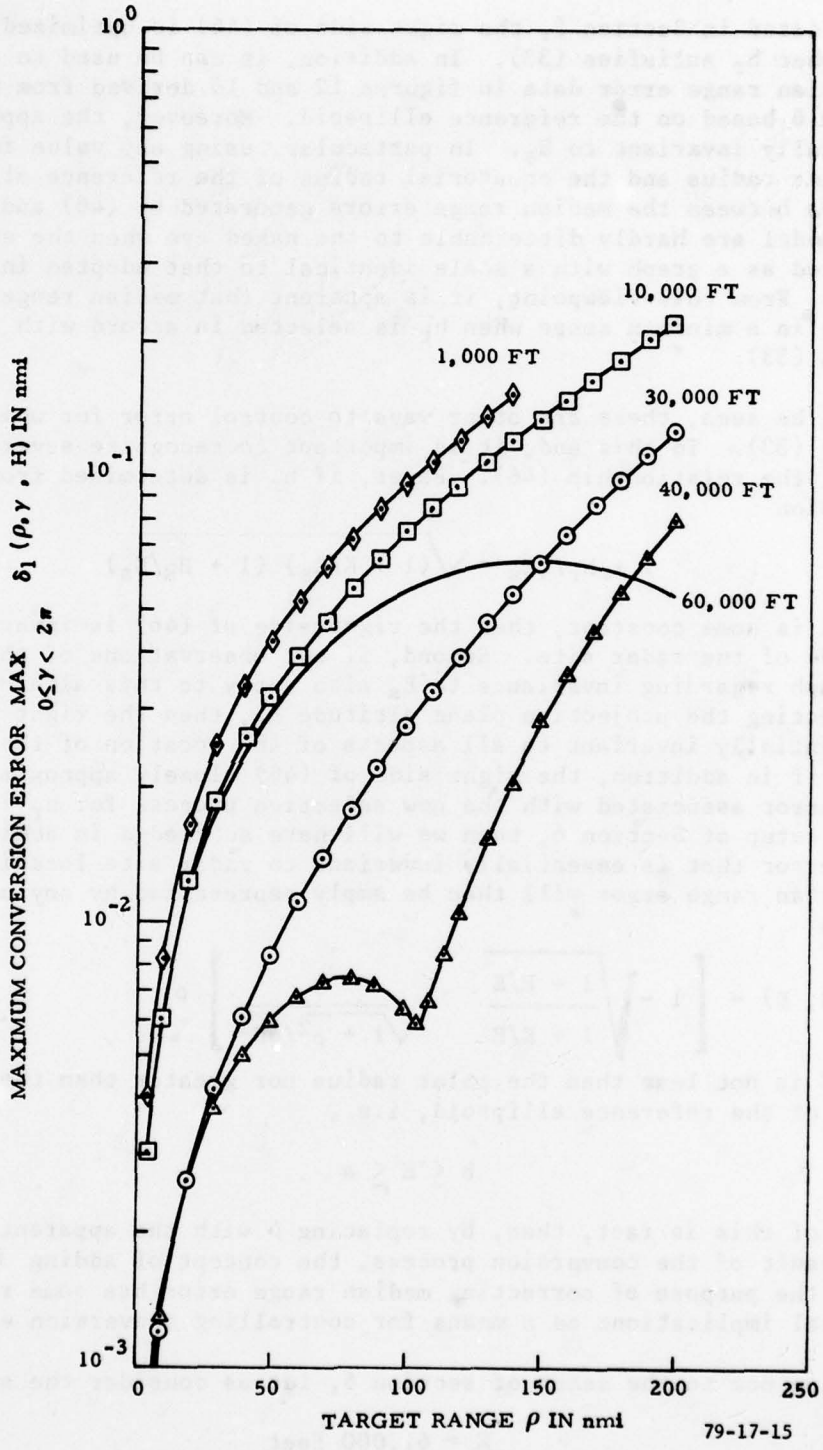

FIGURE 15. MAXIMUM CONVERSION ERROR FOR RADAR AT 10,000 FEET ON PARALLEL 38

As indicated in Section 5, the right side of (46) is optimized in a minimax sense when h_r satisfies (33). In addition, it can be used to approximate the median range error data in figures 12 and 13 derived from the setup of Section 6 based on the reference ellipsoid. Moreover, the approximation is essentially invariant to E_s. In particular, using any value for E_s between the polar radius and the equatorial radius of the reference ellipsoid, differences between the median range errors generated by (46) and the ellipsoidal earth model are hardly discernable to the naked eye when the errors are exhibited as a graph with a scale identical to that adopted in figures 12 and 13. From this viewpoint, it is apparent that median range error is controlled in a minimax sense when h_r is selected in accord with the formula (33).

As will be seen, there are other ways to control error for which h_r does not satisfy (33). To this end, it is important to recognize several characteristics of the relationship (46). First, if h_r is determined from the expression

$$1 + h_r/2E_s = \sqrt{(1 + K/E_s)\ (1 + H_R/E_s)} \tag{47}$$

where K is some constant, then the right side of (46) is invariant to the altitude of the radar site. Second, if our observations of the preceding paragraph regarding invariance to E_s also apply to this alternative method of selecting the projection plane altitude h_r, then the right side of (46) is essentially invariant to all aspects of the location of the radar site. Third, if in addition, the right side of (46) closely approximates the median range error associated with the new selection process for h_r in the context of the setup of Section 6, then we will have succeeded in achieving a median range error that is essentially invariant to radar site location. In fact, the median range error will then be amply represented by any one of the numbers

$$f(\rho, H, E) = \left[1 - \sqrt{\frac{1 + H/E}{1 + K/E}} \qquad \frac{1}{\sqrt{1 + \rho^2/4E^2}}\right] \rho \tag{48}$$

where E is not less then the polar radius nor greater than the equatorial radius of the reference ellipsoid, i.e.,

$$b \leq E \leq a \quad . \tag{49}$$

If all of this is fact, then, by replacing ρ with the apparent range ρ_c observed as a result of the conversion process, the concept of adding $f(\rho_c, H, E)$ to ρ_c for the purpose of correcting median range error has some rather obvious practical implications as a means for controlling conversion error.

Returning now to the setup of section 6, let us consider the situation where

$$K = 61{,}000 \text{ feet} \tag{50}$$

and the projection plane altitude satisfies (47). Figure 16 depicts the median range error as a function of target range and altitude when the radar site is at mean sea level on parallel 38. We have purposely neglected to exhibit the location of the radar in the illustration. The reason is that when similar curves are plotted on the same graph paper for other radar site locations, differences are not discernible to the naked eye. In particular, only differences less than .001 nautical mile were observed among radar site locations at all six combinations of parallels 28, 38, and 48 and altitudes of 0 and 10,000 feet. Moreover, in all these cases, plots of amplitudes of target range oscillations appear as copies of figure 11, and actual numerical differences are less than a few tenths of one meter. In addition, as pointed out earlier, angle error is strictly invariant to the projection altitude h_r so that figure 10 represents the angle errors in the immediate situation. Thus, except for some rather minute perturbations, the sole result of choosing the projection plane altitude in accordance with (47) is the creation of a functional relationship between median range error, target range, and target altitude that is invariant to the latitude and altitude of the radar site. Moreover, it can be readily verified that the functional relationship is extremely well represented by the expression (48) for any constant value of E satisfying the constraint (49). In other words, the desiderata of the preceding paragraph have been realized, and, in addition, it is clear that figures 10 and 11 represent upper bounds on the residual error after the median range error has been removed.

Turning to figure 16, it is apparent that $|\rho - \rho_c|$ will be a good deal less than 1 nautical mile under rather practical limitations on target range ρ and target altitude H. From the same figure, it appears that the corresponding difference between $f(\rho, H, E)$ and $f(\rho_c, H, E)$ is quite small compared to $f(\rho, H, E)$. The obvious conclusion is that median range error can be essentially eliminated by letting

$$z_c' = [\rho_c + f(\rho_c, H, E)]\varepsilon^{i\gamma_c} \tag{51}$$

represent target position in the z-plane instead of z_c (see (34) and (41)). Moreover, we expect that $a_2(\rho, H)$ of figure 11 is very close to being an upper bound on the absolute value of the range error after correction, i.e., the difference between the moduli of z_c' and z. Finally, since the argument of z_c' is the same as that of z_c, the bounds of figure 10 apply to the absolute value of the angle error after correction, i.e., the difference between the arguments of z_c' and z.

From the standpoint of implementation, correction might best be accomplished by means of a polynomial approximation to (48). Along these lines, the Taylor Remainder Formula can be used to show that

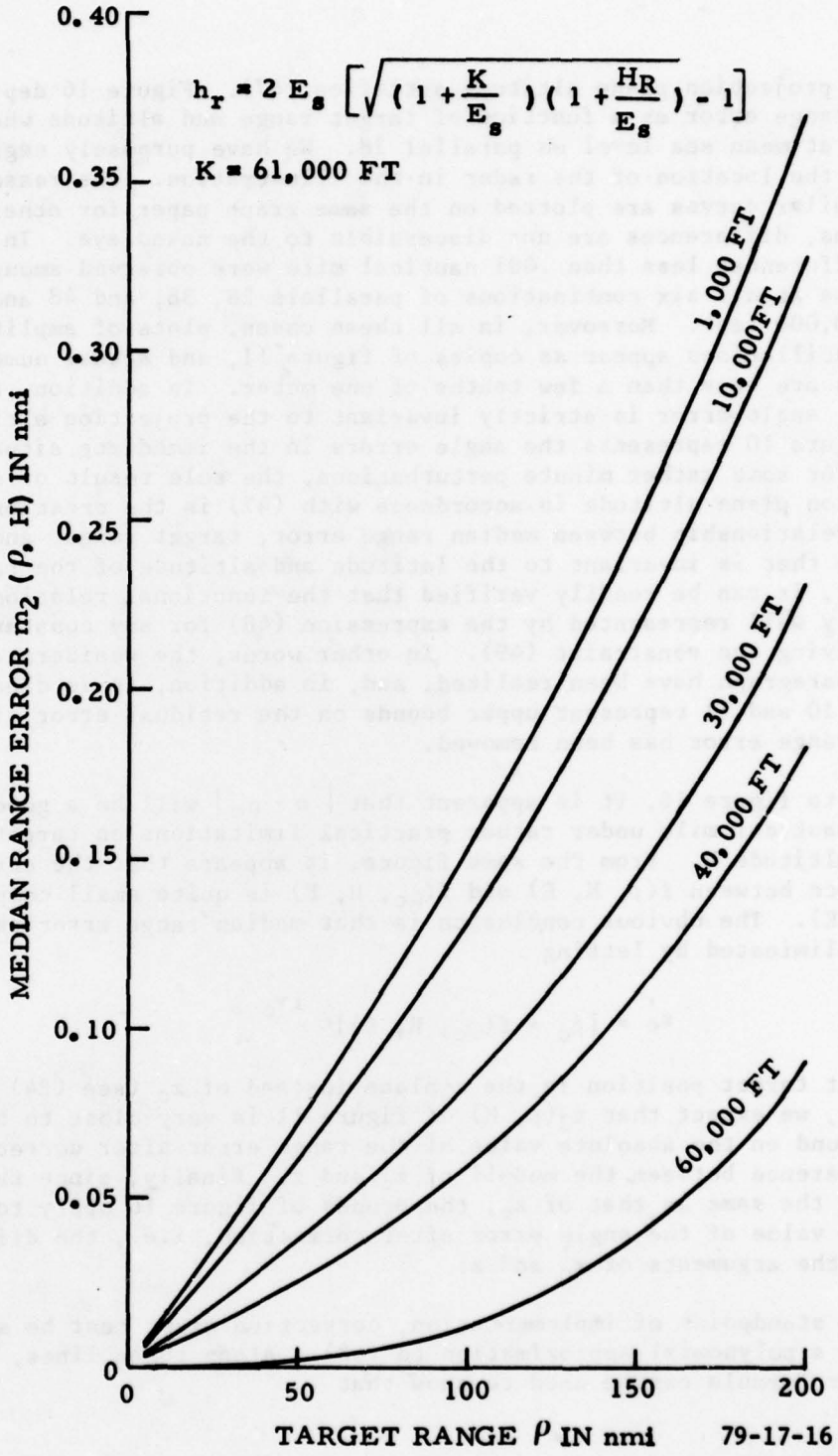

FIGURE 16. MEDIAN RANGE ERROR CORRECTION DATA

$$f(\rho, H, E) = \rho - \frac{\rho}{\sqrt{1 + K/E}} \left[1 + H/2E - \rho^2/8E^2 + \varepsilon(\rho, H, E)\right] \tag{52}$$

where

$$|\varepsilon(\rho, H, E)| \leq 1.5 \times 10^{-6} \tag{53}$$

whenever $\rho \leq 200$ nautical miles, $H \leq 60{,}000$ feet, and E satisfies (49). Thus letting

$$f_o(\rho, H, E) = \rho - \frac{\rho}{\sqrt{1 + K/E}} \left[1 + H/2E - \rho^2/8E^2\right] \tag{54}$$

error correction can be accomplished by adding $f_o(\rho_c, H, E)$ to ρ_c without a significant change in the final outcome due to approximation error.

As pointed out in Section 6, z_c is a function of target range ρ, target angle γ, and target altitude H. Consequently, the conversion error after correction with the cubic approximation (54) can be viewed as a function of these three parameters and E, i.e.,

$$\delta_1'(\rho, \gamma, H, E) = |z - [\rho_c + f_o(\rho_c, H, E)]\epsilon^{i\gamma_c}|. \tag{55}$$

The maximum of this error with respect to γ is illustrated in figure 17 for a radar at sea level on parallel 38 and a target at 60,000 feet. The value of the parameter E has been taken to be the polar radius of the reference ellipsoid in this example. Actually, the conversion errors after correction shown in figure 17 are greater than those observed for targets at altitudes less than 60,000 feet. Moreover, as expected, in all cases the errors are lower bounded by the range error oscillation amplitude. Conversion errors after correction corresponding to the case where the radar site altitude is 10,000 feet are essentially identical to those obtained in the situation where the radar is at sea level. For this reason, the altitude of the radar site does not appear in figure 17. Hence, figure 17 can be viewed as representing upper and lower bounds on conversion error after correction for tanget altitudes not exceeding 60,000 feet. Insofar as the size of conversion error is concerned, a comparison of figure 17 with figures 14 and 15 indicates that error correction offers some advantages as an error control device that cannot be realized with the minimax method.

While the correction approach to error control does seem to offer some advantage over the minimax method, the practicality of the procedure is still a moot question. For example, we have compared the two methods under the assumption that slant range, altitude, and azimuth are known exactly. It remains to consider the situation in which there is measurement error. In addition, we have restricted ourselves to the case where K is 61,000 feet. In the face of measurement error, this may not be the best choice for K. Finally, there may be other limitations imposed by hardware and software considerations.

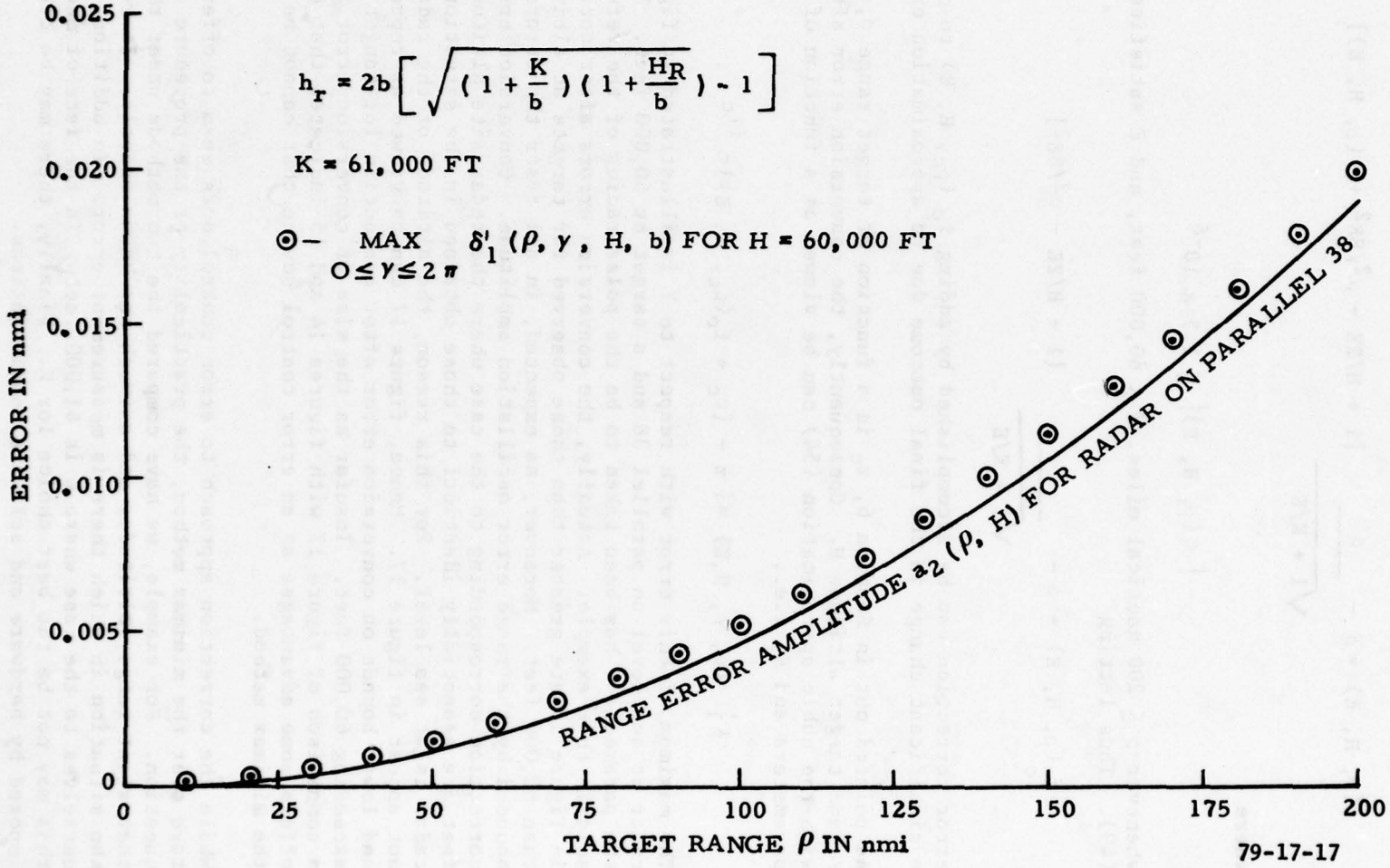

FIGURE 17. MAXIMUM CONVERSION ERROR AFTER CORRECTION FOR RADAR ON PARALLEL 38

9. CONCLUDING REMARKS

Numerical results have been obtained for conversion errors in the context of an earth model based on the reference ellipsoid. Radar locations between parallels 28 and 48 at altitudes between 0 and 10,000 feet were considered. Attention was directed to targets at altitudes from 1,000 to 60,000 feet. Differences between geodetic and conformal latitudes were taken into account. Results have been presented in terms of ranges and angles measured in the local stereographic projection plane with the projection of the radar site location taken as the origin of coordinates. Target ranges from 5 to 200 nautical miles were considered.

At constant target range and altitude, both conversion range and angle errors can be viewed as oscillatory functions of target angle. The median of an angle error oscillation is 0, whereas the median of a range error oscillation is dependent upon target range and target altitude. The amplitude of an angle error oscillation is invariant to radar site altitude and the local projection plane height. This is also essentially true in the case of the range error amplitude. In addition, its dependence on target altitude is negligible. On the other hand, both amplitudes increase monotonically with target range, and angle error amplitude is essentially a nondecreasing function of target altitude. For radar site locations between parallels 28 and 48 at altitudes from 0 to 10,000 feet, results indicate that angle error amplitude is upper bounded by a linear function of target range assuming the values of .00025° and .0056° at target ranges of 5 and 200 nautical miles, respectively. By the same token, range error amplitude is upper bounded by a convex up curve that is essentially 0 at a target range of 5 nautical miles and increases to 0.0195 nautical miles at a target range of 200 nautical miles.

The height of the local stereographic projection plane was determined by two methods. One of these corresponds to a minimax approach to error control based on a spherical earth model. The other gives rise to another approach for reducing conversion error. In the case of the minimax procedure, the median of a range error oscillation is invariant to radar site latitude. On the other hand, it is strongly dependent upon the altitude of the site. In the case of the alternative approach to error control, it is essentially invariant to all aspects of radar site location thereby providing a set of universal error correction curves.

In the case of the minimax procedure, the overall conversion error can reach 0.08 nautical mile for a radar at sea level on parallel 38. If the site is raised to 10,000 feet, errors as large as 0.22 nautical mile are possible. In the case of the alternative approach to error control, results indicate that the overall conversion error can be reduced considerably. In fact, numerical results indicate that the overall conversion error is essentially reduced to the level of the range error oscillation amplitude. Cubic approximations to error control curves derived from this approach appear to be capable of restricting the overall conversion error to within 2 meters of this level. However, the practicality of the approach is a moot question.

In conclusion, it must be emphasized that we have considered conversion errors under the assumption that sensor measurements are exact and data processing is carried out with infinite precision. In practice, this is not the case. Receiver front-end noise exists, range and azimuth measurements are quantized before being passed on to the central processor, trigonometic functions and other mathematical relationships are approximated in various ways, and multiplication, addition, etc., are carried out using finite precision arithmetic. All of these contribute to error, and we have no reason to believe that the effect upon the conversion process is inconsequential. In this sense, our results might be viewed as representing lower bounds for conversion error that are attainable only under ideal operating conditions.

REFERENCES

1. Goldenberg, D., and Wolf, E., A Common Coordinate System for the Utilization of Data from Several Radars, Lincoln Laboratory, Lexington, Mass., Technical Report No. 67, September 1954.

2. Wolf, E., A Stereographic Coordinate System for the Utilization of Data from Several Radars, The MITRE Corporation, Bedford, Mass., Report No. SR-2, March 1959.

3. Gingerich, E., Stereographic Projections in Air Traffic Control Systems, Journal of the Institute of Navigation, Volume 24, No. 2, Summer 1977.

4. Flax, B., Coordinate Conversion and Coordinate Transformation in the National Airspace System, Institute of Transportation and Traffic Engineering, University of California, Berkley, California, Report submitted in fulfillment of Course CE-299, August 1975.

5. Tveitan, W., An Introduction to the Radar Data Collection Coordinate Processing and Display Functions in SAGE, The MITRE Corporation, Bedford, Mass., Working Paper W-3648 (Appendix A), April 1961.

6. Abramowitz, M., and Stegun, I., Handbook of Mathematical Functions, National Bureau of Standards, Washington, D.C., 1966.

7. Mulholland, R. and Stout, D., Numerical Studies of Conversion and Transformation in a Surveillance System Employing a Multitude of Radars - Part II, Report No. FAA-NA-79-18, National Aviation Facilities Experimental Center, Atlantic City, N.J., April, 1979.